Regional and hemispheric impacts of anthropogenic and biomass burning emissions on summertime CO and O₃ in the North Atlantic lower free troposphere

R. E. Honrath,[1] R. C. Owen,[1] M. Val Martín,[1] J. S. Reid,[2] K. Lapina,[1] P. Fialho,[3] M. P. Dziobak,[1] J. Kleissl,[1] and D. L. Westphal[1]

[1] We report summertime measurements of CO and O₃ obtained during 2001–2003 at the PICO-NARE mountaintop station in the Azores. Frequent events of elevated CO mixing ratios were observed. On the basis of backward trajectories arriving in the free troposphere and global simulations of biomass burning plumes, we attribute nearly all these events to North American pollution outflow and long-range transport of biomass burning emissions. There was a high degree of interannual variability in CO levels: median [CO] ranged from 65 ppbv in 2001 to 104 ppbv in 2003. The highest concentrations were associated with transport of Siberian fire emissions during summer 2003, when Siberian fire activity was unusually high. Ozone mixing ratios also increased (by up to ∼30 ppbv) during the fire events. These findings demonstrate the significant hemispheric scale impact that biomass burning events have on background CO and O₃ levels. O₃ enhancements of similar magnitude were also observed in North American pollution outflow. O₃ and CO were correlated during North American outflow events, with a slope averaging 1.0 (d[O₃]/d[CO], ppbv/ppbv) when no fire impact was present. This slope is more than 80% larger than early 1990s observations made in the eastern United States and nearshore outflow region, even after accounting for declining U.S. CO emissions and for CO loss during transport to the Azores, and is not consistent with simple dilution of U.S. outflow with marine background air. We conclude that a significantly larger amount of O₃ production occurred in the air sampled during this study, and we suggest several potential reasons for this, each of which could imply potentially significant shortcomings in current estimates of the hemispheric impact of North American emissions on tropospheric ozone and should be evaluated in future studies. *INDEX TERMS:* 0365 Atmospheric Composition and Structure: Troposphere—composition and chemistry; 0368 Atmospheric Composition and Structure: Troposphere—constituent transport and chemistry; 0345 Atmospheric Composition and Structure: Pollution—urban and regional (0305); 0322 Atmospheric Composition and Structure: Constituent sources and sinks; *KEYWORDS:* tropospheric ozone, North Atlantic, biomass burning

1. Introduction

[2] In this paper, we present summertime measurements of ozone and carbon monoxide made at the PICO-NARE station, a mountaintop observatory in the Azores Islands. The Azores Islands provide an ideal location to investigate North American export of primary pollutants and the export and potential en-route production of ozone. They are located south of the dominant warm conveyor belt export pathway, an export route that has been analyzed extensively [*Cooper et al.*, 2001; *Eckhardt et al.*, 2004]. However, they are frequently impacted by large scale flow patterns in the lower troposphere, which export summertime North American emissions and carry them to the Azores approximately 5 to 7 days later. In addition, they are frequently exposed to outflow from arctic and subarctic regions, which can transport emissions from biomass burning in Canada, Alaska, and Siberia.

[3] Quantification of the impacts of these emissions on tropospheric ozone at the continental to global scale is of great interest for several reasons. Ozone is estimated to be the third most important greenhouse gas [*Houghton et al.*, 2001] and is the primary source of tropospheric hydroxyl radical. In addition, it is damaging to agricul-

[1]Department of Civil and Environmental Engineering, Michigan Technological University, Houghton, Michigan, USA.

[2]Marine Meteorology Division, Naval Research Laboratory, Monterey, California, USA.

[3]Group of Chemistry and Physics of the Atmosphere, University of the Azores, Angra do Heroismo, Portugal.

tural crops and forests at levels not greatly above current background levels in many regions [*Mauzerall and Wang*, 2001; *Fowler*, 1999], and human health impacts, of concern in ozone precursor source regions, are affected by the background levels to which locally produced ozone is added.

[4] It is difficult or impossible to use direct measurements to quantify the increase in hemispheric background ozone levels resulting from a specific region's emissions. However, several studies have observed intercontinental transport of plumes containing elevated ozone before they have dispersed to background levels. These include observations in Europe of ozone produced from North American emissions [*Trickl et al.*, 2003], of ozone from Europe in Asia [*Pochanart et al.*, 2003], and of Asian ozone in North America [e.g., *Parrish et al.*, 1992; *Jaffe et al.*, 1999]. These observations have demonstrated the occurrence of large-scale anthropogenic impacts on ozone, but the long transport distances involved and the presence of emissions from the downwind continent make clearly detectable intercontinental transport an infrequent event.

[5] Measurements of the quantity of ozone and ozone precursors exported from an upwind continent can also be used to assess hemispheric impacts. Such measurements have been the focus of many studies, such as the PEM, NARE and TRACE campaigns [e.g., *Banic et al.*, 1996; *Hoell et al.*, 1997; *Jacob et al.*, 2003]. Global chemical transport models (GCTMs) predict that more than half of the ultimate ozone impact of continental anthropogenic emissions results from ozone production over the continent and the nearshore downwind region [e.g., *Li et al.*, 2004]. The additional downwind ozone production resulting from export of nitrogen oxides (NO$_y$) can be estimated using GCTMs, with model estimates of NO$_y$ export evaluated using measurement-based export estimates (from North America [e.g., *Stohl et al.*, 2002; *Li et al.*, 2004; *Parrish et al.*, 2004]). However, model simulations of the exported nitrogen oxides' fate and impact on ozone production well downwind are somewhat uncertain, due to the inadequate density of nitrogen oxides measurements in remote regions. Measurements of ozone enhancements in well aged exported continental airmasses provide one method to assess these processes.

[6] Carbon monoxide measurements are used in this study for two purposes. In studies of the ozone enhancement resulting from anthropogenic emissions, simultaneous measurements of carbon monoxide are useful as CO is a long-lived tracer of primary emissions [e.g., *Parrish et al.*, 1993]. In addition, at the hemispheric and global scale CO plays an important role in tropospheric chemistry as a major sink of OH [*Thompson*, 1992] and a source of peroxy radicals. Interannual variability in background CO levels is significant, largely as a result of variations in the magnitude of biomass burning [*Wotawa et al.*, 2001; *Novelli et al.*, 2003], and measurements of CO at a remote location such as the central North Atlantic provide information on the emission events that ultimately disperse to create that background.

[7] The PICO-NARE measurements are analyzed here with two main objectives: to characterize the degree to which North American anthropogenic emissions and North American and Siberian biomass burning emissions (and variations in the frequency of transport of those emissions over the Azores) affect CO levels in the Azores region, and to characterize the associated enhancement in O$_3$ and the resulting implications for North American impacts on regional and hemispheric ozone levels.

2. Methods
2.1. Station

[8] The PICO-NARE station is located at an altitude of 2225 m, on the summit caldera of Pico mountain, an inactive volcano on Pico Island in the Azores, Portugal (38 degrees, 28.226 min north latitude, 28 degrees, 24.235 min west longitude). This temporary station was established in July 2001 and has been operating since then, with the exception of power outages and instrument downtime. Access to the summit is limited to a strenuous trail and is impossible at some times of year, due to snow- and ice-cover and inclement weather. For this reason, all measurements are fully automated. The station is powered by a diesel generator located approximately 2.5 km away and approximately 1000 m lower in altitude.

[9] Since subtropical marine boundary layers are typically between 800 and 1600 m deep and stratocumulus-topped [*Albrecht et al.*, 1995], one might expect the station to be constantly in the free troposphere (FT). However, orographic effects on atmospheric flow have been of importance to other maritime, mountain-based observatories (e.g., daytime upslope flow at Mauna Loa [*Mendonca*, 1969], and thermal internal boundary layers at Santa Barbara mountain on Terceira island in the Azores [*Peterson et al.*, 1998]). Unique topographic features of Pico mountain, such as its high altitude (2225 m MSL) and strong slope (~50% between z = 1200 m and z = 2200 m) make it relatively resistant to penetration of marine boundary layer air to the altitude of the PICO-NARE station. While some rising of streamlines as they approach the mountain is expected [*Ding et al.*, 2003], the topographic features noted above, the short upwind fetch (<12 km for prevailing winds from SW to NE), and typical stable stratification above the marine boundary layer (MBL) (buoyancy frequency $N \sim 1.4\ s^{-1}$ based on radiosonde observations taken at Lajes on nearby Terceira island) suggest a small vertical displacement. These arguments are confirmed by comparing meteorological measurements at the PICO-NARE station to radiosonde data from Lajes (distance 118 km ENE), which show that airmasses at the same height as the PICO-NARE station have properties very similar to those observed at the station. Personal experience from spending many days at the station also suggests that the lowest layer of stratocumulus clouds is frequently situated well below the mountain summit. Finally, backward trajectories calculated in the marine boundary layer do not appear to explain the high-CO events observed at the station (see below). Thus, we expect that the measurements presented here mainly characterize the lower free troposphere, though marine boundary layer air is probably sampled at times. (The extent to which these expectations

are correct will be evaluated using meteorological measurements made along the slope of Pico mountain during summer 2004.)

2.2. Measurements

[10] Carbon monoxide measurements: Carbon monoxide was determined using a commercial instrument (Thermo Environmental, Inc., Model 48C-TL), modified by the addition of a palladium catalyst (0.5% Pd on alumina) operated at 250°C to remove CO while passing water vapor and by the addition of a mass flow controller, as described by *Parrish et al.* [1994]. The instrument alternated between 2 min of zero measurement and 2 min of ambient measurement; the first minute of each mode was discarded to ensure equilibration. Instrument sensitivity was determined daily by standard addition at the inlet to increase the CO mixing ratio by approximately 600 ppbv. Measurements during calibration were zeroed and analyzed identically to those during other times. Three different CO standards (Scott Specialty Gases, Troy, MI) were used. These were intercompared to one another and to a fourth standard (Scott-Marin, Riverside, CA), which was referenced to the current [*Novelli et al.*, 2003] NOAA CMDL standard (personal communication, P. Novelli, NOAA CMDL, 2003); all agreed within the manufacturer-specified uncertainties. Uncertainty in the calibration standards' mixing ratios (4.0 to 4.4% in the 188.3 to 191.3 ppm standards) and mass flow controller flow uncertainty (2% for the calibration gas flow controller and 4% for the sample flow controller based on bubble flowmeter calibration) result in potential bias of ±6%, relative to the CMDL CO standard. Instrument sensitivity (volts/ppbv) was stable over long periods; it varied by ±3% (total range of variation) over the period July 2001–August 2003, after adjusting for occasional changes to instrument output range settings. Five-day running averages of the nightly sensitivity determinations were used to improve precision when reducing the data. The resulting sensitivity estimates have precision better than 1%. Measurement precision (2-σ) was ±8 ppbv or better. The 30-min averages used in most of the analyses presented here average 7 to 8 one-min-average points, and have 2-σ precision of ±3 ppbv or better.

[11] Ozone measurements: Ozone was measured with commercial ultraviolet absorption instruments (Thermo Environmental Instruments Inc., Franklin, Massachusetts; Model 49C). Daily tests were conducted to verify stability of the zero reading and to identify ozone loss in the inlet filter or inlet line, if present. Activated carbon-scrubbed ambient air was sampled to measure the zero reading; the presence of inlet loss was evaluated by adding ozone generated by the instrument's internal ozonator at the inlet and, alternatively, inside the instrument, bypassing the inlet line. During the periods for which ozone data are reported here, the zero reading was constant and equal to the instrument zero setting within the manufacturer-specified measurement precision (1 ppbv), and inlet loss was not detectable (≳2%).

[12] Ingestion of water through the ozone inlet contaminated the instrument during the winter of 2001–2002, and residual, unrecognized damage from that event resulted in the loss of all summer 2002 ozone measurements. The sensor was fully repaired in spring 2003 and was replaced with a new instrument of the same model in summer 2003. (The addition of heated inlet funnels prevented a recurrence of the problem.)

[13] The ozone measurements reported here were referenced to the NIST reference standard using the following methods. The ozone instrument used in 2001 (and early summer 2003) and a portable ozone sensor (ultraviolet absorbance technique; 2B Technologies Inc., Boulder, Colorado, Model 202) were compared with a NIST-referenced NOAA CMDL network ozone standard (S. Oltmans, NOAA CMDL, personal communications, 2001, 2002). Prior to the start of the study, the instrument used during summer 2001 produced ozone readings 3.9 ± 0.3% low, relative to the NIST-referenced CMDL instrument. The portable sensor was used to check the slope of both instruments during early summer 2003, and the two TEI instruments were also intercompared at that time. The comparison of the 2001 instrument to the portable sensor was consistent with the pre-study CMDL comparison. The comparisons of the two TEI instruments indicated that the 2003 instrument produced ozone values a further 3.5 ± 0.3% lower than the 2001 instrument; the comparison of the 2003 instrument with the portable sensor was consistent with this result. Based on these comparisons, we have adjusted our ozone measurements to the NIST reference as follows: all measurements were multiplied by 1.039, and those made with the 2003 instrument were multiplied by an additional factor of 1.035.

[14] Ozone measurements were recorded as 1-min averages. Measurement precision, as indicated by twice the standard deviation of the 60 1-s measurements included in each average, was usually less than 1 ppbv. Higher variability, which is believed to reflect true variations in the ambient ozone mixing ratio but could indicate worsened measurement precision, occurred only rarely (e.g., 2.5% of the 1-min average values were based on 1-s measurements with standard deviations exceeding 1 ppbv). In this paper, we have further averaged in 30-min blocks for analysis of the correlation between O_3 and CO.

2.3. Backward Trajectories

[15] Trajectories were calculated with the Hybrid Single-Particle Lagrangian Integrated Trajectories (HYSPLIT) model [*Draxler and Rolph*, 2003] using meteorological data from the National Weather Service's National Center for Environmental Prediction (NCEP) FNL data set [*Stunder*, 1997]. The data are available every 6 hours on a 129 by 129 point hemispheric stereographic grid with output on 13 mandatory pressure levels and the surface level. Backward trajectories were calculated every six hours. At these times, a set of six trajectories was initiated: one terminating at the station, four terminating at end points separated by 1° of latitude and longitude from the station, and one terminating directly below the station, at a height of 2000 m. Trajectories were run for 10 days backward in time, with trajectory locations recorded every hour. In addition to these trajectories, a second set of five backward trajectories ending directly below the first set, at a height of 200 m, was calculated

for comparison of flow pathways in the marine boundary layer with those in the lower free troposphere.

2.4. Biomass Burning Emissions and Transport Modeling

[16] To help identify periods potentially impacted by biomass burning plumes, we examined posted simulations from the NRL Aerosol Analysis and Prediction System (NAAPS) coupled with the Fire Locating and Modeling of Burning Emissions (FLAMBE) aerosol forecast system. This global aerosol forecasting system is run in near real time and provides 5 day forecasts of sulfate, smoke and dust. Data are posted on two NRL web sites (http://www.nrlmry. navy.mil/aerosol/ and http://www.nrlmry.navy.mil/flambe/). A complete discussion of these tools is outside the scope of this manuscript, but relevant aspects and references are presented here.

[17] The NAAPS global model is a modified form of a hemispheric model of sulfate aerosols developed by *Christensen* [1997]. NAAPS uses global meteorological analysis and forecast fields from Navy's Operational Global Analysis and Prediction System (NOGAPS) [*Hogan and Brody*, 1991] on a 1 by 1 degree global grid, at 6-hour intervals and 24 vertical levels reaching 100 mb. Dust and smoke emissions, transformations and sinks have been added to the model. NAAPS is made up of three components: data gathering and quality control, data assimilation, and transport modeling. Twice daily, the NOGAPS weather forecast model provides dynamical fields to NAAPS at 6-hour intervals for the five-day forecast period. Dry and wet deposition is derived from the NOGAPS fields. Unlike the sources of other aerosol components, which are wind driven (e.g., dust and sea salt) or prescribed in a seasonal inventory (e.g., fossil fuel combustion), biomass-burning emissions have significant daily variability that defies easy parameterization. For timely forecasting, fluxes must be generated within 12 hours of emissions. Real-time fire hot spot monitoring by satellite is the only available method to construct a smoke flux for such a model. The FLAMBE project does this by integrating fire hot spot analyses from two satellite systems into the forecast model. For the western hemisphere, the GOES 8/10/12 geostationary Wildfire Automated Biomass Burning Algorithm (WF_ABBA) is utilized [*Prins et al.*, 1998, 2001, 2003]. The GOES 8/10/12 WF_ABBA is a modified version of the South American ABBA that has been used to monitor biomass burning in South America since 1995. For the rest of the globe, the twice-daily MODIS fire product is used [*Justice et al.*, 2002].

[18] To compute fluxes, half-hourly WF_ABBA and twice daily MODIS fire products are assigned smoke particle flux rates in 9 land cover sub-categories derived from the 1 km USGS-derived Global Land Cover Characteristics (GLCC) classification (http://edcdaac.usgs.gov/glcc/glcc.html) (e.g., boreal forest or swamp/marsh lands). These fluxes are a function of estimated fuel load, emission factors, and combustion fractions. For WF_ABBA, fire products are directly assimilated into the NAAPS source function algorithms. For MODIS products, a static diurnal cycle is imposed based on characterizations from North America WF_ABBA analyses. Specifics and references are listed on the FLAMBE web site provided above and elsewhere [*Reid et al.*, 2004b, 2004a]. These emissions are injected into the lowest 1 km of the model atmosphere.

[19] The largest difficulty in assigning fluxes from fire hotspot analysis is knowing fuel loadings and burned areas. Based on global land use algorithms, some accounting can be made. Even so, *Reid et al.* [2004b, 2004a] found a tremendous free parameter space from which to generate emissions. Biases form in region-specific ways. In this manuscript, we estimate interannual differences in smoke production. Because work on regional calibration factors is ongoing, the FLAMBE team suggests that fluxes be taken qualitatively. Following this recommendation, we use the fluxes (below) to assess temporal changes on a region-specific basis.

[20] To confirm interannual variability in emissions, we also utilize satellite-derived burn scar data from the Global Fire Monitoring Center (http://www.fire.uni-freiburg.de). While this method cannot track individual emissions episodes at high temporal resolution, the method probably offers the most consistent means of identifying interannual differences in regional burning.

3. Results and Discussion

3.1. Carbon Monoxide Observations

[21] Time series of CO measurements each year are shown in Figure 1; Figure 2 compares the distributions of CO mixing ratios observed each year. A significant degree of interannual variability is present. Bimodal distributions were observed in 2001 and 2003 (Figure 2a), but the peaks were shifted 20 ppbv or more higher in 2003; the 2002 distribution was monomodal, with a peak between those in 2001 and 2003. The cumulative probability distributions shown in Figure 2b highlight these differences. For example, the 50th percentile (the median) increased from 65 ppbv in 2001 to 80 ppbv in 2002 and 104 ppbv in 2003. Large interannual variability in hemispheric and global CO levels is known to occur, and has been attributed to variations in biomass burning emissions [*Wotawa et al.*, 2001; *Novelli et al.*, 2003]; the impact of biomass burning on the present observations is discussed below. In contrast, the minimum CO levels observed each year were quite similar at approximately 50 ppbv. This minimum, which is associated with transport of well aged marine air (see below), is lower than that observed in the marine boundary layer of the nearby Azores island of Terceira in 1993 [*Parrish et al.*, 1998] (shown with the dotted line in Figure 2b), which exhibited a lower limit of 65–70 ppbv. This difference may reflect a decadal decline in northern hemisphere CO emissions [*Parrish et al.*, 2002; *Novelli et al.*, 2003], possibly in combination with a small enhancement of MBL CO levels due to local or regional emissions, as was observed for nitric oxide at the same location [*Peterson et al.*, 1998].

[22] The two modes of the bimodal distributions observed in 2001 and 2003 and the single mode of the 2002 distribution are indicated with vertical lines in Figure 2. These modes will be used below and referred to as "low-CO" and "high-CO" modes.

[23] As a first step toward identification of the source of the high-CO mode, we conducted a backward trajectory residence time analysis [*Poirot and Wishinski*, 1986]. In this analysis, the distribution of trajectory residence times above
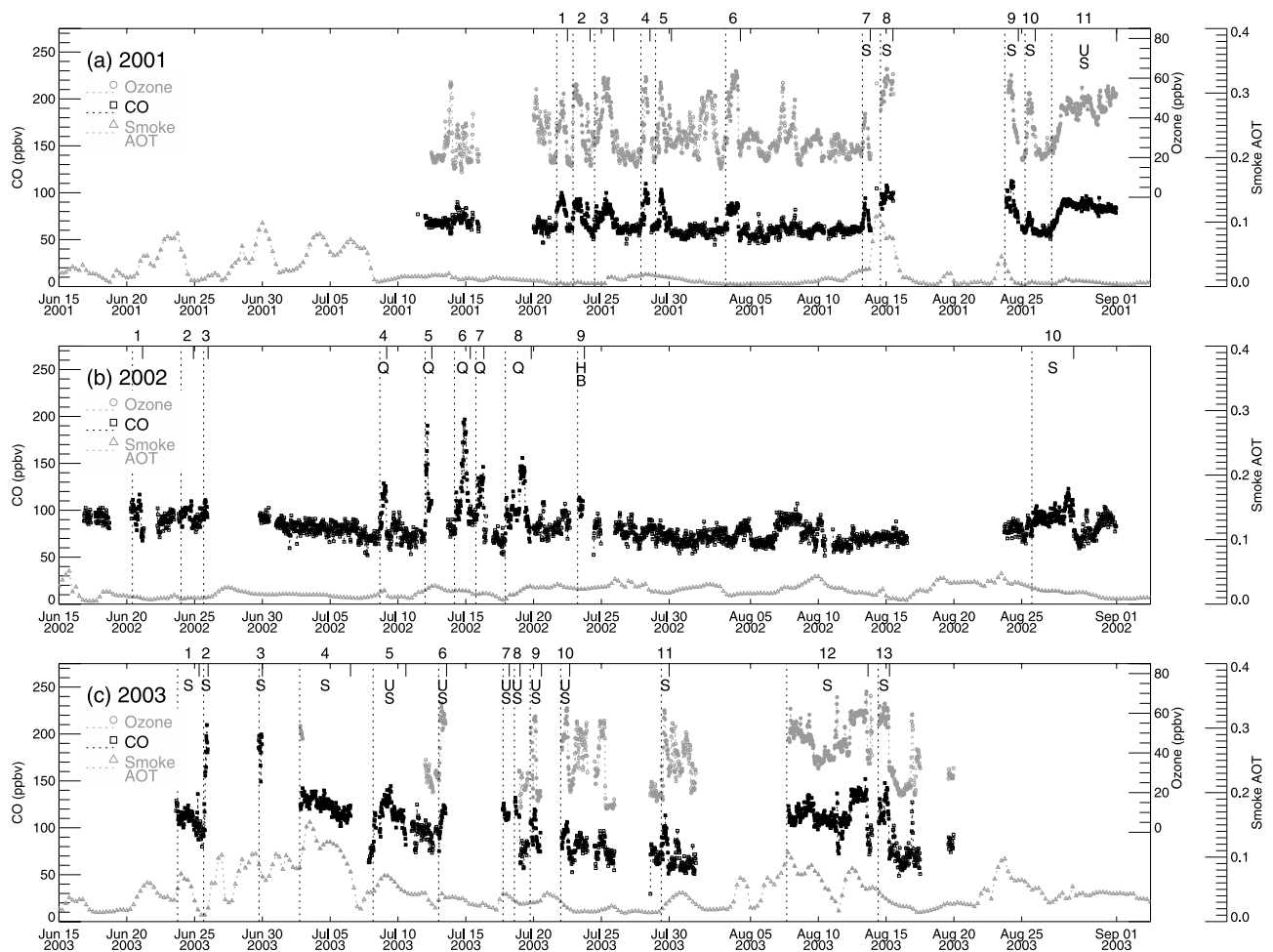
Figure 1. Time series of measured CO, measured O$_3$, and NAAPS/FLAMBE smoke aerosol optical thickness (AOT) each summer. CO is plotted with red squares, ozone is plotted with blue circles, and smoke AOT is plotted with black triangles. (Ozone measurements are not available during summer 2002, and are missing during some periods in 2003.) Events discussed in the text begin at the dotted vertical lines, end at the solid vertical lines, and are numbered above each plot; values during these events are plotted with solid symbols. Source-fire regions for biomass burning-impacted periods (discussed in section 3.1.2) are identified near the top of each plot: S, Siberia; Q, Quebec; HB, Hudson Bay; US, the western United States. See color version of this figure at back of this issue.

each point on the map was calculated by summing the number of hourly endpoints in 1 degree by 1 degree grid cells and normalizing by the area of each grid cell. Each normalized sum was then multiplied by a geometric correction factor [*Merrill*, 1994] proportional to the distance of each grid cell from the PICO-NARE station, such that a random distribution of trajectory endpoints would result in equal values of the geometrically corrected residence time at each cell. The results are shown in Figure 3 for analyses of back-trajectories arriving at all measurement times (left column of Figure 3), as well as those arriving at the times of CO mixing ratios below the low-CO mode (middle column of Figure 3) and those arriving at times of CO mixing ratios above the high-CO mode (right column of Figure 3). In the case of 2002, which did not have a high-CO mode, a value of 20 ppbv above the CO mode of 76 was used for Figure 3f.

[24] Comparison of the results obtained during high-CO and low-CO periods indicates that high CO observations are

associated with higher frequencies of flow over the northeastern U.S. (in 2001 and 2003) and regions just offshore (2002), over the region east and west of Florida (2001), over the midwestern U.S. (2003), and over sparsely populated regions of Canada (2002 and 2003). (Note that Figure 3 is designed to identify regions associated with high-CO observations each year, but is not ideal for the comparison of flow patterns between years; an analysis designed for that purpose is presented at the end of the next section, 3.1.1.)

[25] To illustrate the apparent influence of anthropogenic and biomass burning emissions in these regions with more precision, we next analyze transport pathways during individual high-CO periods. This is followed by a discussion of the influence of biomass burning emissions on interannual variability and individual high-CO periods.

3.1.1. Analysis of High-CO Events

[26] Events of elevated CO were arbitrarily defined as periods when CO levels exceeded the low-CO mode plus 20 ppbv. This method of identification was used to avoid
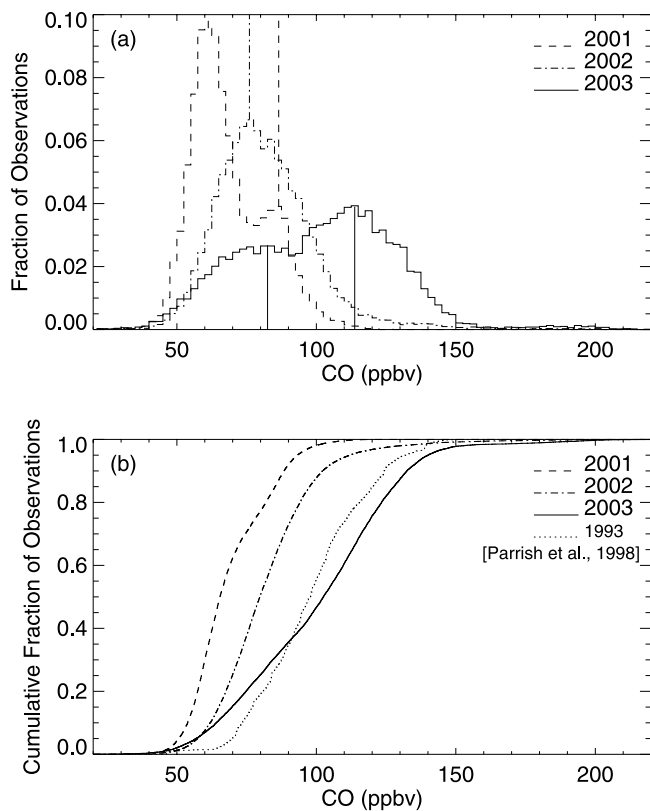
Figure 2. (a) Histograms and (b) cumulative probability distributions of summertime CO observations during 2001, 2002, and 2003. Vertical lines in Figure 2a indicate the low-CO and high-CO modes (see text). The 1993 measurements made by *Parrish et al.* [1998] in the marine boundary layer on the nearby island of Terceira are also shown in Figure 2b.

bias that could result from subjective choice of events. (However, it may result in the omission of some periods influenced by North American emissions, which, as shown below, are characterized by relatively small CO enhancements but relatively large O_3 enhancements.) These high-CO events are identified in Figure 1.

[27] Backward trajectories arriving at 2.2 km altitude during the high-CO portion of each event were analyzed and used to classify the event according to potential source regions. The resulting classifications are summarized in Table 1 (column titled "Source") and were selected as follows. Events during which some or all of the trajectories passed through the lower 2 km of the continental U.S. or Canada south of 48° N were classified as U.S. boundary layer (abbreviated as USBL in Table 1), to indicate the potential influence of surface emission sources during these events. Events with trajectories that passed over the same regions of North America but not in the lower 2 km were classified as U.S. free troposphere (abbreviated USFT). Events with trajectories that passed over the region east of the U.S. and north of the Caribbean islands, but which did not cross the North American continent, were classified as far western Atlantic (WAtl). Events with trajectories that passed over Canada, usually but not always in the lower 2 km of the atmosphere, were classified as northern North America (N-NA). Finally, two events with trajectories that

travelled from the north, east of Canada, were classified as North. These region classifications were applied if any of the six backward trajectories arriving each 6 hours during the high-CO portion of each event passed over a given region. Finally, many trajectories travelled from central Canada and then over the U.S.; in these cases, the event was classified as both USBL and N-NA. Examples of typical backward trajectories associated with the most common source classifications are shown in Figures 4a–4n. (In addition, Figures 4o and 4p show flow during a typical low-CO period for comparison.) Backward trajectories arriving in the marine boundary layer below the station are also shown in Figure 4. In almost all cases, trajectories travelling in the MBL during these high-CO periods did not pass over emission regions.

[28] Nearly all of the high-CO events occurred during periods of flow from the U.S. boundary layer, the far western Atlantic region, and/or northern North America. Most events in 2001 were associated with flow from the U.S. boundary layer or the far western Atlantic, while most in 2002 and 2003 occurred during flow from the U.S. boundary layer or northern North America. Enhanced CO levels during periods of flow from the U.S. boundary layer (e.g., Figures 4a, 4e, 4i, and 4m) are expected, due to the high emission intensity in that region. Similarly, events with far western Atlantic flow (Figures 4c and 4g) are likely attributable to North American emissions as well, as the backward trajectories, which neglect atmospheric dispersion, pass rather close to the southeastern U.S. However, the observed CO enhancement during periods of flow from northern Canada (e.g., Figure 4k) is not attributable to anthropogenic emissions. CO levels during these N-NA periods included the highest observed, suggesting a significant impact from biomass burning emissions, which are analyzed in the next section.

[29] While this analysis of the trajectory pathways associated with observed CO enhancements is useful for the determination of apparent CO source regions, it is insufficient for assessment of the contribution that variations in transport may have made to the interannual variability of CO levels discussed above (Figure 2). For this purpose, we categorized the backward trajectories arriving at the times of all CO measurements each summer (i.e., not just high-CO periods), and compare, in Table 2, the fractions of trajectory arrival times each year for which (a) any trajectories (of the six calculated at each arrival time) pass through the USBL region, (b) any trajectories pass through the N-NA region, and (c) all six calculated trajectories remain over the North Atlantic Ocean (20–60°W, 14–45°N) during their entire 10-day lifetime. (Also shown in Table 2 are the numbers of hours of CO samples that each of the fractions corresponds to.)

[30] The results indicate that the measurements during summer 2003 included significantly more periods of N-NA flow and USBL flow than did those in 2001, in combination with a reduction in the frequency of clean marine flow. During 2002, N-NA flow was much less frequent than in 2003, but still occurred at a 50% higher frequency than in 2001. In addition, the greater CO data coverage during 2002, relative to 2001, also contributed to a larger number of observations during periods of USBL and N-NA flow in 2002 (relative to 2001). Thus, differences in
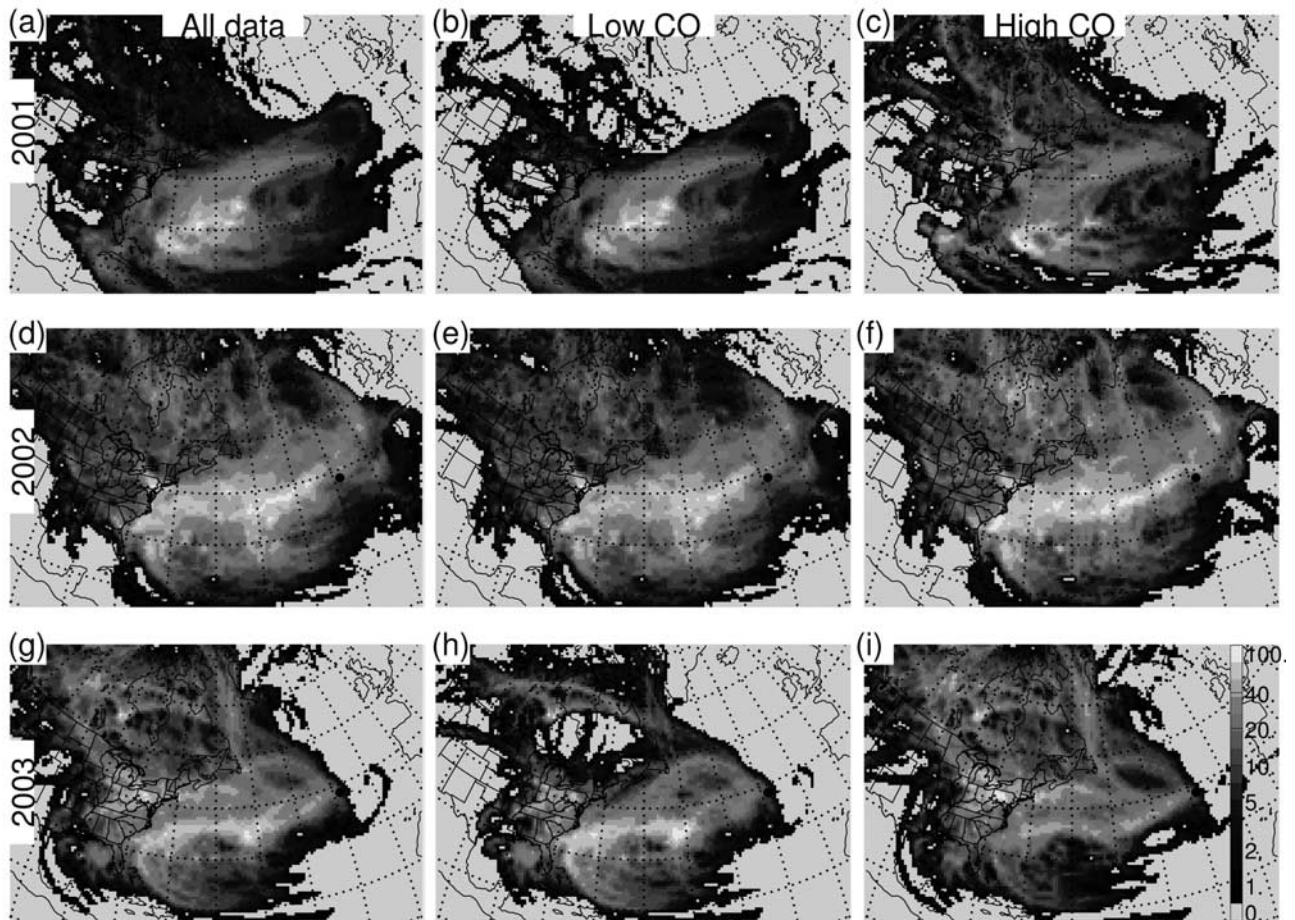
Figure 3. Residence time plots for (a, d, g) all data each summer, (b, e, h) low-CO periods (see text for definition), and (c, f, i) high-CO periods (see text for definition) during (a, b, c) 2001, (d, e, f) 2002, and (g, h, i) 2003. Color scale (shown in Figure 3i) is normalized to the highest geometrically corrected residence time value in each data subset. See color version of this figure at back of this issue.

the number of hours of periods with flow through the USBL and N-NA regions probably contributed to the interannual variability in CO levels apparent in Figure 2, especially the more frequent observations of high CO levels in 2003 and more frequent observations of low CO levels in 2001. However, as discussed in the next section, interannual variability in biomass burning emissions also played a significant role.

3.1.2. Biomass Burning Impacts

[31] In this section, we assess the contribution of biomass burning to CO enhancements observed during the high-CO events. First, however, we discuss its contribution to the high degree of interannual variability in CO observed at Pico (i.e., the low CO levels during 2001 and the high CO levels during 2003).

[32] Interannual variability: Interannual variability of emissions is assessed using the MODIS fire product, the WF_ABBA geostationary fire product, and the Freiburg burn scar product, as described in section 2.4. Each of these data sets has advantages and disadvantages. However, all vary consistently during our study period, and by considering them together we are able to construct a coherent picture of fire emissions.

[33] When analyzing interannual variability, consistency in the flux estimation methods used throughout the period of study is of primary importance. Absolute biomass-burning emission products must be developed on a region-specific basis [*Reid et al.*, 2004b, 2004a], because they are calibrated on a region-by-region basis. Therefore, we separately examine each major source region in the northern hemisphere: Siberia, eastern Europe, and northern North America.

[34] Figure 5 shows the global distribution of fire emissions produced by the FLAMBE project (based on GOES and MODIS images) during the summers of 2001–2003; these emission estimates are also used in the NAAPS model simulations presented below. The day-by-day variations in emissions are shown in Figure 6. (To avoid potential bias in interannual trends, we have used only Terra MODIS fire data in developing the emission estimates shown in Figure 6. This is necessary because the Terra satellite covers our entire period of study, while the Aqua satellite does not; inclusion of Aqua MODIS data would have biased the later data because of the timing of the Aqua overpass, which coincides with the diurnal peak in burning intensity. In contrast, Figure 5 is designed to show the regions
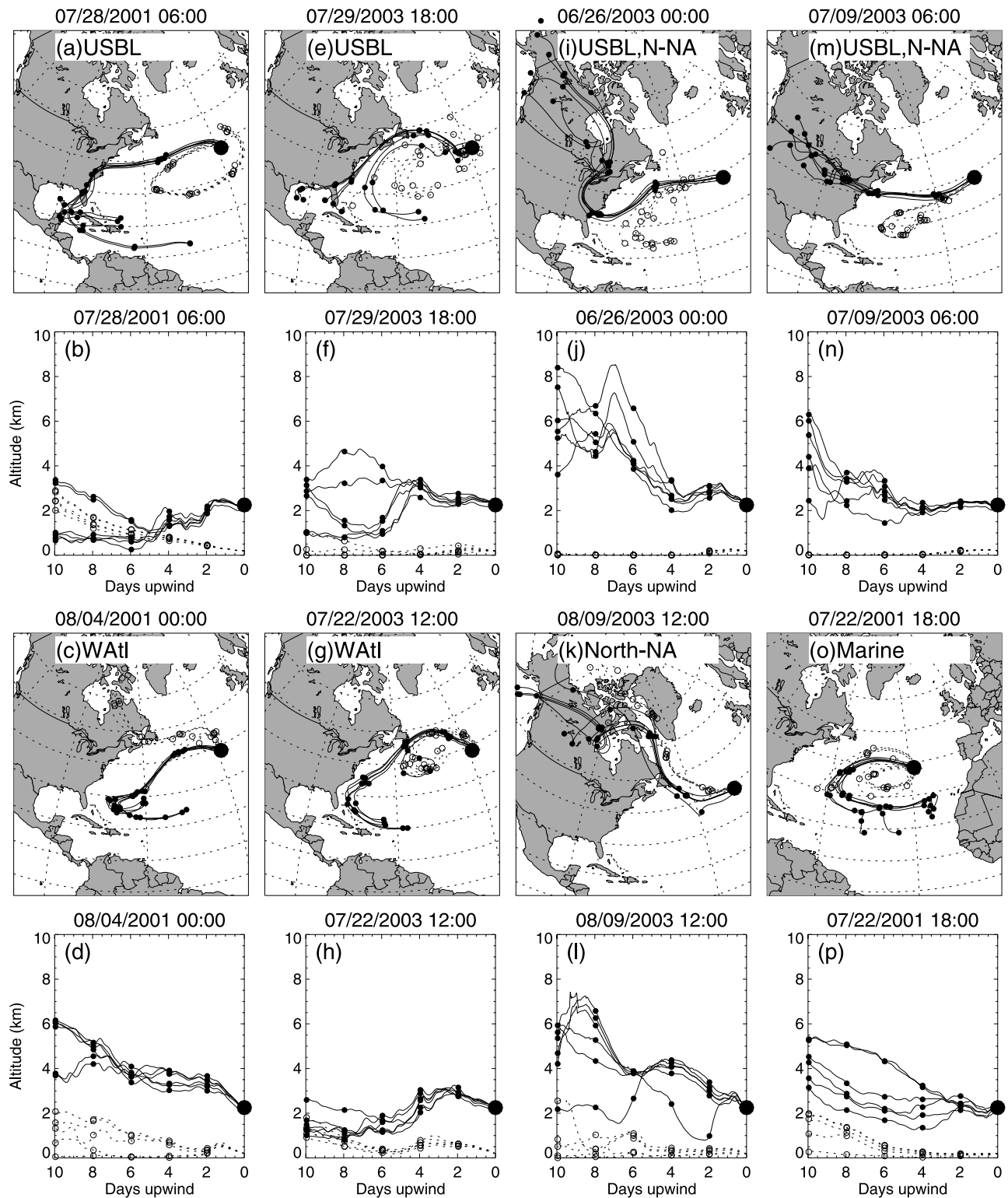
Figure 4. Typical backward trajectories for the transport pathways listed in Table 1. Solid lines show the paths of the six trajectories ending on a grid around and immediately below the station location; dotted lines show trajectories ending in the marine boundary below the station. Trajectory arrival times are listed above each pair of plots. (a, e, i, m) and (c, g, k, o) Horizontal paths of the trajectories. (b, f, j, n) and (d, h, l, p) Their altitude profiles. Small dots mark each 2 days travel time. The location of the PICO-NARE station is shown with a large dot.

Table 1. Summary of Events Identified in Figure 1

Event	Period	Source[a]	BB[b]	Slope[c]	r^{2} [d]	N[e]
Year 2001						
1	July 21 17:00–July 22 12:00	N-NA,USBL		$0.82^{+0.12}_{-0.11}$	0.76	37
2	July 22 22:00–July 24 04:00	WAtl		$1.21^{+0.12}_{-0.11}$	0.83	58
3	July 24 12:00–July 25 22:00	N-NA,USBL/Watl		$1.28^{+0.48}_{-0.35}$	0.53	67
4	July 27 22:00–July 28 14:00	USBL		$0.92^{+0.09}_{-0.08}$	0.83	24
5	July 29 00:00–July 30 04:00	N-NA,USBL		$0.81^{+0.17}_{-0.14}$	0.68	55
6	Aug. 3 04:00–Aug. 4 06:00	WAtl		$1.22^{+0.17}_{-0.15}$	0.77	51
7	Aug. 13 06:00–Aug. 13 20:00	USBL	S	$0.79^{+0.09}_{-0.08}$	0.81	20
8	Aug. 14 14:00–Aug. 15 12:00	N-NA	S	$0.92^{+0.38}_{-0.27}$	0.51	31
9	Aug. 23 18:00–Aug. 24 18:00	N-NA,USBL	S	$0.91^{+0.45}_{-0.30}$	0.45	35
10	Aug. 25 06:00–Aug. 26 00:00	USBL,WAtl	S	$1.52^{+0.27}_{-0.23}$	0.72	35
11	Aug. 27 05:00–Sep 01 00:00	N-NA,USBL/WAtl	US	$1.12^{+0.52}_{-0.36}$	0.46	225
All				$0.96^{+0.35}_{-0.26}$	0.53	638
Year 2002						
1	June 20 10:00–June 21 04:00	USBL				0
2	June 24 00:00–June 24 22:00	North				0
3	June 25 16:00–June 26 00:00	North				0
4	July 08 16:00–July 09 04:00	N-NA,USBL	Q			0
5	July 12 00:00–July 12 12:00	N/A	Q			0
6	July 14 04:00–July 15 08:00	N-NA,USBL	Q			0
7	July 15 18:00–July 16 08:00	N-NA,USFT	Q			0
8	July 17 22:00–July 19 20:00	N-NA	Q			0
9	July 23 06:00–July 23 18:00	N-NA	HB			0
10	Aug. 25 18:00–Aug. 28 20:00	N-NA,USFT	S			0
All						0
Year 2003						
1	June 23 18:00–June 25 08:00	N-NA	S			0
2	June 25 16:00–June 26 00:00	N-NA,USBL	S			0
3	June 29 18:00–June 30 00:00	N-NA,USBL	S			0
4	July 02 18:00–July 06 12:00	N-NA,USBL	S			9
5	July 08 04:00–July 10 14:00	N-NA,USBL	US			0
6	July 13 00:00–July 13 14:00	N-NA,USBL	US	$0.87^{+0.29}_{-0.22}$	0.57	25
7	July 17 18:00–July 18 05:00	N-NA,USBL	US			0
8	July 18 14:00–July 19 00:00	N-NA,USBL	US			2
9	July 19 18:00–July 20 14:00	N-NA,USFT,WAtl	US	$1.13^{+0.07}_{-0.06}$	0.89	33
10	July 22 00:00–July 22 16:00	WAtl,N-NA	US	$1.05^{+0.07}_{-0.06}$	0.88	29
11	July 29 10:00–July 30 00:00	USBL	S	$0.89^{+0.37}_{-0.26}$	0.50	27
12	Aug. 7 16:00–Aug. 13 16:00	N-NA	S	$0.64^{+0.31}_{-0.21}$	0.45	276
13	Aug. 14 10:00–Aug. 15 06:00	N-NA	S	$0.42^{+0.25}_{-0.15}$	0.40	37
All				$0.65^{+0.31}_{-0.21}$	0.46	438

[a]Source, source region classification, described in the text. N/A, no backward trajectories were calculated during high-CO portions of the event.

[b]BB, biomass burning. Entries in this column indicate events potentially impacted by biomass burning plumes, with the letter indicating the region of the source fire emission. S, Siberia; Q, Quebec; HB, Hudson Bay; US, the western United States.

[c]Slope, geometric mean regression slope. Not shown for events missing most O_3 measurements. Uncertainties indicate range of ordinary least squares slopes, as described in the text.

[d]r^2, correlation coefficient squared. Not shown for N < 5.

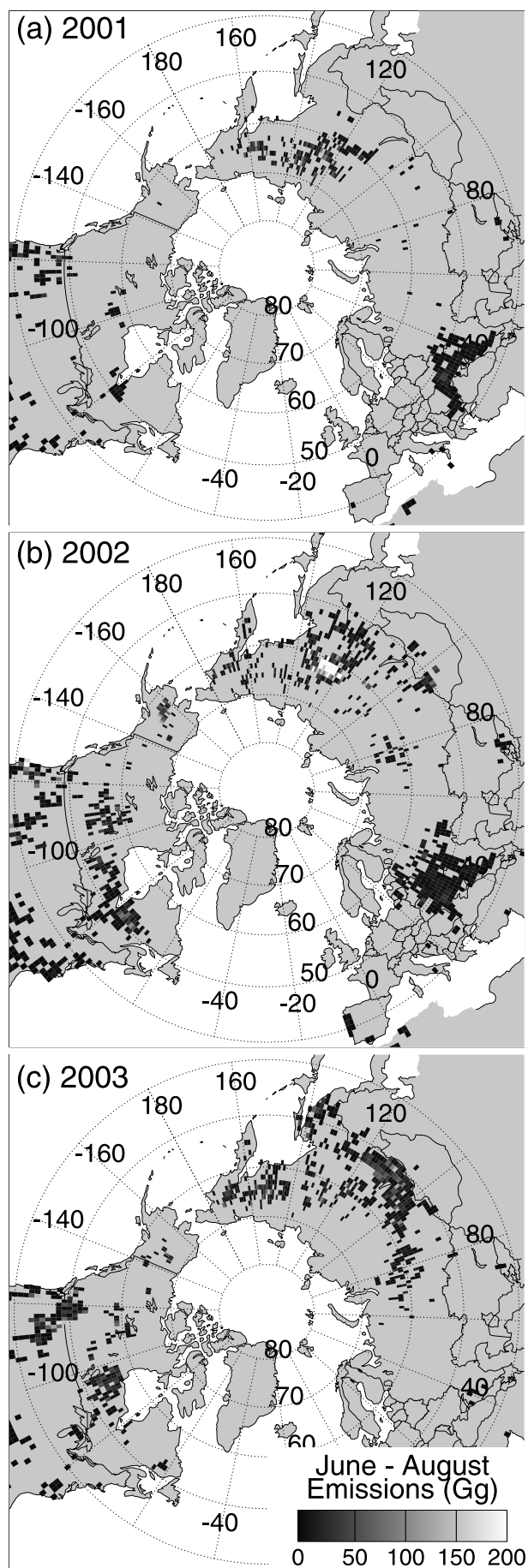[e]N, number of simultaneous 30-min average CO and O_3 measurements.

responsible for emissions each year, rather than interannual differences, and therefore includes Aqua data.) While these figures display particulate emissions estimates, they are based on the application of smoke-particle emission factors to estimates of burn areas by land cover type, as discussed above, and variations in the estimated fluxes are driven by variations in the rate of fuel combustion. As a result, we expect the temporal variation of CO emissions to approximately follow that of particles; recent analyses of Australian fire emissions support this expectation [*Paton-Walsh et al.*, 2004].

[35] In the eastern Europe/western Asia region, Siberia typically experiences 3 to 6 times the emissions of eastern Europe, and is therefore expected to be the dominant regional source. In 2001, Siberian emissions were low and sporadic (Figure 6). Emissions were higher in 2002, and the highest FLAMBE emissions were calculated in 2003. The high 2003 emissions were mainly due to record burning during May and June (Figure 6) in the Lake Baikal region

(Figure 5). Later in the summer of 2003, fire activity shifted to the northeast, with significant emissions north of the Kamchatka Peninsula. The low 2001 and high 2003 FLAMBE emissions are supported by satellite-derived burn scar area estimates (Global Fire Monitoring Center, 2003, http://www.fire.uni-freiburg.de/) of 10 million ha burned in Siberia in 2000, 8 in 2001, 12 in 2002, and 19 in 2003 [*Jaffe et al.*, 2004, Figure 2]. In eastern Europe, the interannual variability was somewhat different, with large sets of fires in

Table 2. Frequency of Backward Trajectory Flow Through the Indicated Regions and Number of Hours of Corresponding CO Measurements, as Described in the Text

Year	USBL		N-NA		Marine	
	%	hours	%	hours	%	hours
2001	24.3	209.	5.0	43.	30.3	260.
2002	21.5	280.	7.2	94.	32.1	418.
2003	46.8	326.	21.0	146.	15.2	106.

Figure 5. The spatial patterns of summertime biomass burning aerosol particle emissions during (a) 2001, (b) 2002, and (c) 2003 from the real-time FLAMBE emission model. See color version of this figure at back of this issue.

the Moldova region in 2001 and 2002, and little emission in 2003.

[36] In northern North America, 2001 was also a quiet fire year relative to 2002 and 2003 (Figure 6c). In 2001, the principle fires of note were in Idaho, near the Canadian border (Figure 5). During 2002, fire activity increased in the boreal regions of Canada, with one very large event in Quebec. The Quebec fires (∼July 5, 2002) produced massive emissions, causing optical depths above 8 and significant degradation of air quality in the northeastern U.S. coast region [*Eck et al.*, 2003; *Colarco et al.*, 2004; *Pahlow et al.*, 2004]. Emissions increased further in 2003, with large sustained fires south of Hudson Bay, as well as large fires in Idaho and Montana. Thus, the interannual variability of North American fire emissions tracked that of Siberian emissions during our study period.

[37] Given that boreal biomass burning CO emissions are estimated to be similar in magnitude to total U.S. and European anthropogenic emissions even in average fire years [*Wotawa et al.*, 2001], we conclude that the high 2003 CO levels observed at Pico were the result of greatly enhanced fire emissions from Siberia, and of moderately enhanced North American fire emissions. This conclusion is supported by CO column measurements by the MOPITT instrument on the Terra satellite: *Edwards et al.* [2004] report zonal mean CO columns throughout the northern latitudes during spring-summer 2003 that were the highest in the 2000–2003 MOPITT data record. They attribute the high values to the spring and late-summer Siberian fires, and note that CO column enhancements in transported plumes from the Lake Baikal fires were large enough that they could be tracked as far east as the eastern United States. Significant impacts of these fires on ground-level CO concentrations in the northwestern U.S. have also been reported [*Jaffe et al.*, 2004].

[38] High-CO events: In contrast to tropical and subtropical burning, which is fairly steady during the typical burning season [*Reid et al.*, 2004b, 2004a], Northern Hemisphere burning emissions are quite episodic (Figure 6). Most fire events, indicated by the separate spikes in the figures, last under 10 days. Most apparent in Figure 6 are the Lake Baikal event in May–June 2003 and the Moldova fires in August 2002. In northern North America (Figure 6c), the Quebec fires in July 2002 and those in the Hudson Bay region in August 2003 stand out.

[39] The episodic nature of northern fire emissions results in the formation of separate fire plumes that can be transported long distances. Figure 1 shows the resulting NAAPS simulation of aerosol optical thickness (AOT) above the PICO-NARE station due to biomass burning emissions. Since AOT can result from the passage of aerosol plumes above the station, we do not expect to see CO enhancements coincident with each AOT peak. In addition, NAAPS incorporates aerosol wet deposition and surface deposition, which do not significantly affect CO, so the relative enhancement in biomass smoke AOT and
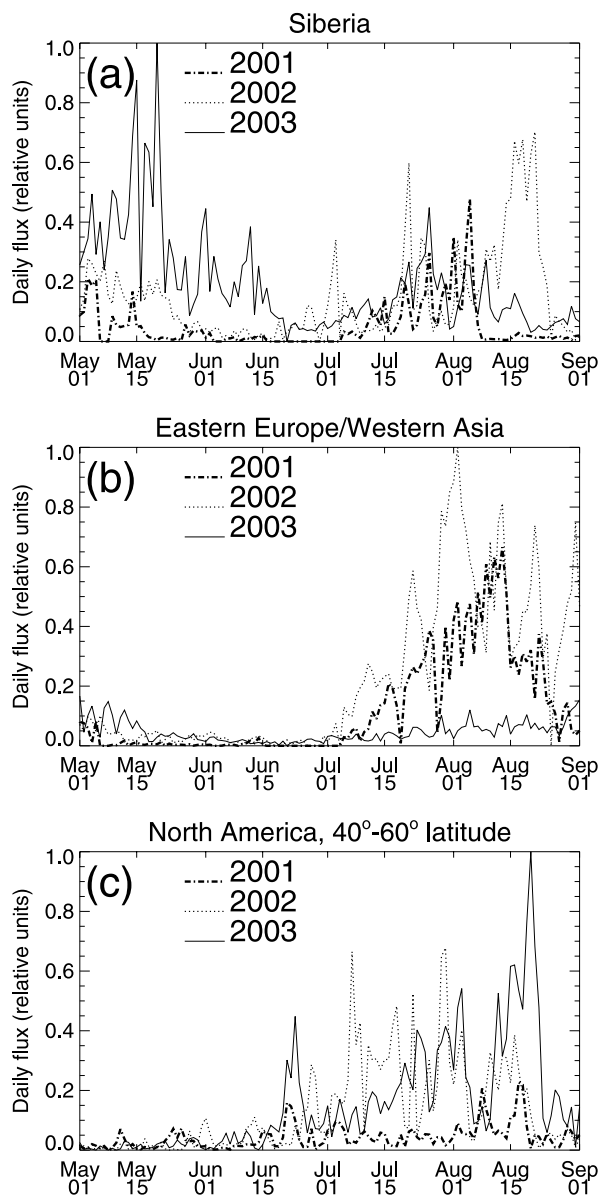
Figure 6. Relative daily FLAMBE emissions for (a) Siberia, (b) eastern Europe and western Asia, and (c) northern North America for 2001–2003. Each plot is scaled to the maximum daily emission for the region shown over the period January 2001 to December 2003.

biomass-derived CO is expected to vary, depending on airmass history. Nevertheless, peaks in AOT indicate a potential impact of biomass burning emissions, and examination of Figure 1 indicates correlation between AOT and CO enhancements in many cases.

[40] By inspecting NAAPS output showing the long-range transport of smoke puffs, we have attributed the AOT enhancements in Figure 1 to the dominant source fires responsible. During summer 2001, the only significant AOT enhancements during the CO measurement period occurred in mid- to late August, as a result of early August fires in Siberia and (in event 11) fires in Idaho. The enhanced smoke AOT over the Azores coincided with moderate CO enhancements. During 2002, the plume from the Quebec

fires reached the Azores during high-CO events 4–8 and coincided with the highest CO levels observed that summer. Continued burning in the Hudson Bay area is responsible for elevated AOT calculated through the end of July, and may have been responsible for high-CO event 9. Finally, a plume from a Siberian fire reached the Azores in August; high-CO event 10 occurred during the end of this event. Fire impacts of varying magnitude are simulated during all 2003 high-CO events. Emissions from the May–June record-size Lake Baikal fires reached the Azores during events 1–4. Events 3 and 4 resulted from the last major emission events from this fire group. The emission plume travelled for more than 2.5 weeks before reaching the Azores, but coincided with the highest summertime CO mixing ratios observed. During 2003 events 5–10, emissions from U.S. forest fires are responsible for the smoke AOT simulated over the Azores; elevated CO levels correlated to the simulated smoke AOT were observed during events 5–9. Emissions from the second set of 2003 Siberian fires, near the Bering Strait, contributed to simulated AOT over the Azores during high-CO events 11–13; coincident large enhancements in CO occurred during events 12 and 13.

[41] The high-CO events potentially impacted by biomass burning emissions are summarized in Table 1. In many cases, transport of biomass burning emissions over the Azores (indicated in the column titled "BB") coincided with air flow from the North American boundary layer (indicated in the column titled "Source"). This was generally the result of flow patterns of the type shown in Figure 4i, which bring air from higher latitudes over the eastern U.S. and on toward the Azores.

3.1.3. Summary of Deduced Sources of Observed CO Enhancements

[42] In almost all cases, the events identified in Figure 1 are attributable to North American anthropogenic CO emissions or to biomass burning. The only exceptions are 2002 events 2 and 3, which exhibited a relatively small CO enhancement during transport from the north and may have resulted from the latitudinal CO gradient. During 2001, enhancements in CO levels resulted from both North American anthropogenic emissions and Siberian fire emissions, with increases of similar magnitude. The highest CO levels, observed during 2002 and 2003, are all attributable to fire emissions, in Canada during 2002 and in Siberia and the United States during 2003. The importance of anthropogenic emissions during 2002 and 2003 was smaller than in 2001, apparently as a result of the increased biomass burning emissions in 2002, and greatly increased biomass burning emissions in 2003.

3.2. Ozone Enhancement During Events of Elevated CO

[43] Ozone is also plotted in Figure 1, and usually varied with CO during the high-CO events. The correlation between ozone and CO is shown in Figure 7.

[44] The relationship between mixing ratios of O$_3$ and CO in transported regional plumes is believed to be an indicator of the magnitude of net O$_3$ production, normalized by precursor emissions [e.g., *Parrish et al.*, 1993]. This interpretation is based on the approximately linear relationships between CO mixing ratios and integrated CO emissions, between CO emissions and O$_3$ precursor emissions, and
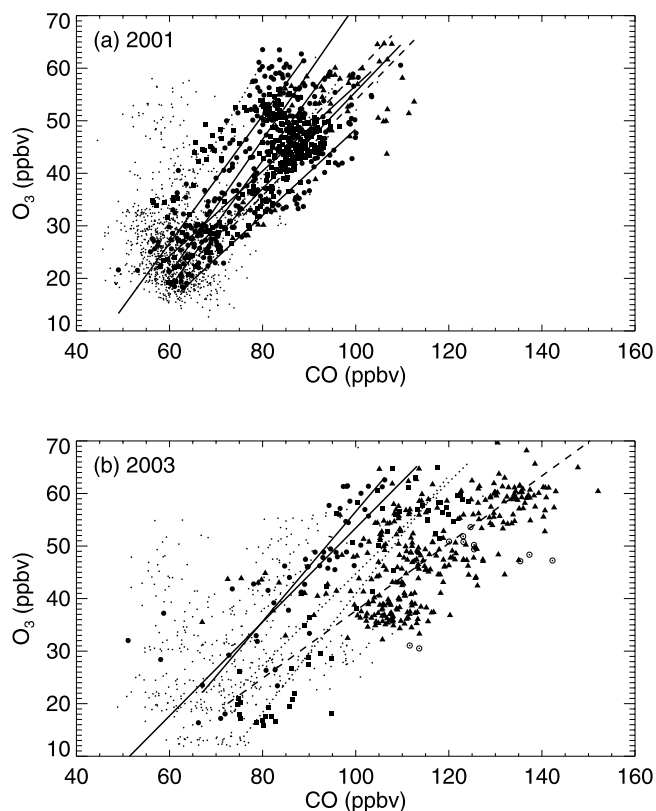
Figure 7. Relationship between CO and O_3 during (a) 2001 and (b) 2003 (O_3 measurements during 2002 are not available). Measurements obtained during periods outside of the events listed in Table 1 are plotted with small black dots. Observations obtained during the events listed in Table 1 are plotted with larger symbols, and regression lines are shown for those events with slope uncertainty below 50%. Symbols and lines are coded according to each event's identified source region and the potential for biomass burning influence, as follows: solid red circles and red solid lines: USBL with no or minimal biomass burning influence (2001 events 1–6, 2003 events 10–11; see text); solid blue triangles and blue dashed lines: biomass burning-influenced periods (not USBL) (2001 events 8–9, 2003 events 12–13); solid green squares and green dotted lines: other (mixed influence) (2001 events 7 and 10–11, 2003 events 6 and 9); and measurements during the small fractions of 2003 events 4 and 8 for which ozone measurements were made: open black circles. See color version of this figure at back of this issue.

between O_3 precursor emissions and integrated net O_3 production. The O_3:CO ratio, as determined by the slope $d[O_3]/d[CO]$, is quite stable in summertime surface measurements in the northeastern U.S.: measurements made in Alabama, Massachusetts, and Pennsylvania during 1988–1992 all produced slopes in the range 0.28–0.32 [*Chin et al.*, 1994]. Measurements at Harvard Forest in eastern Massachussetts are also in this range, but provide evidence that the robustness of the 0.3 value may mask variations in O_3 production efficiency: *Moody et al.* [1998] found that while 1990–1993 summertime (June–August) measurements made at that site exhibited an overall slope of 0.33,

measurements obtained during flow from the west exhibited a significantly higher slope (0.42). They suggested that this difference may have reflected more complete ozone production in the more highly aged air sampled during westerly flow, in combination with an increase in ozone production efficiency resulting from the higher temperatures, higher isoprene levels, and greater insolation under clearer skies that were associated with westerly flow but not southerly or southwesterly flow.

[45] Nevertheless, measurements of $d[O_3]/d[CO]$ slopes in the maritime provinces of Canada, up to 1000 km downwind of the main North American emission sources, exhibit slopes nearly identical to those observed over the northeast U.S., ranging from 0.35–0.45 for monthly slopes based on measurements during June–August of 1991, 1993, and 1991–1994 [*Parrish et al.*, 1998]. (While these slopes are somewhat higher than 0.3, this difference is the result of the use of a two-sided regression technique, rather than the ordinary least squares technique used in prior studies [*Parrish et al.*, 1998].) These slopes are based on measurements at surface stations; a similar slope (0.26) was observed above the boundary layer in aircraft flights sampling air 2–4 days downwind of the eastern U.S. [*Daum et al.*, 1996]. (Summertime CO and O_3 measurements at an Azores marine boundary layer location have also been reported [*Parrish et al.*, 1998]. However, these exhibited poor correlation ($r^2 = 0.24$), suggesting that North American pollution is not clearly detectable in the marine boundary layer of the Azores region during summer.)

[46] Measurements in plumes exported further to the south also indicate slopes of similar magnitude. During the CITE3 study in August–September 1990, *Anderson et al.* [1993] observed $d[O_3]/d[CO]$ slopes averaging 0.4 in plumes exported in the boundary layer off of the region between South Carolina and New Jersey, while *Dickerson et al.* [1995] reported a slope of 0.27 in measurements made at Bermuda during June 1992.

[47] For comparison with these prior observations, slopes were calculated for each of the transport events observed at the Pico station. The results are listed in Table 1 and plotted in Figure 7. These slopes were calculated using the geometric mean (reduced major axis) two-sided regression technique [*Ayers*, 2001; *Draper and Smith*, 1998]. In this method, the calculated slope is equal to the geometric mean of slopes calculated using ordinary linear regression of O_3 against CO and of CO against O_3. Although the uncertainty of the resulting reduced major axis slope estimate is not well defined, the range defined by these two slopes provides an estimate of the uncertainty [*Draper and Smith*, 1998] and is included in Table 1. The calculated slopes are significantly different on average for events impacted by biomass burning (but not U.S. outflow) and those that were not. We therefore discuss these separately, beginning with events not impacted by biomass burning emissions.

3.2.1. U.S. Pollution Transport Events Without Biomass Burning Influence

[48] The slopes observed at Pico during North American pollution transport events were significantly larger than those reported for the eastern U.S. and regions downwind. During 2001, events 1–6 were apparently the result of North American outflow, without significant biomass burning CO. Ozone and CO were highly correlated during these events

Table 3. Comparison of Summertime $d[O_3]/d[CO]$ Slopes Observed at the PICO-NARE Station With Prior Observations in and Downwind of the Eastern United States

Location	Year	Regression Method[a]	Slope Reported	Slope Adjusted	Source
Eastern U.S. BL	1988–1992	one-sided	0.28–0.32		*Chin et al.* [1994]
(adjusted for 20% CO emissions reduction)				0.38	
Harvard Forest, W flow	1990–1993	one-sided	0.42		*Moody et al.* [1998]
(adjusted for 20% CO emissions reduction)				0.53	
Sable Island	1991	one-sided	0.29		*Parrish et al.* [1993]
Sable Island	June 1991–1994	two-sided	0.43		*Parrish et al.* [1998]
	July 1991–1994	two-sided	0.27		*Parrish et al.* [1998]
	Aug. 1991–1994	two-sided	0.34		*Parrish et al.* [1998]
East of Nova Scotia	Aug. 1993	one-sided	0.26		*Daum et al.* [1996]
Sable Island	June–Aug. 1991–1994	two-sided	0.36[b]		*Parrish et al.* [1998]
(adjusted for 20% CO emissions reduction)				0.45	
Pico, USBL flow	June–Aug. 2001, 2003	two-sided	1.0		this work
(CO adjusted back 4 days for comparison with Sable Island)				0.81	
(CO adjusted back 6 days for comparison with the eastern U.S.)				0.73	

[a]Where not specified, slopes are presumed to be obtained using one-sided, ordinary least squares regression.

[b]Calculated using the same regression technique applied to the Pico observations, using all Sable Island data obtained during June, July, and August 1991–1994 (D. Parrish, personal communication, 2002).

($r^2 = 0.53$–0.83); $d[O_3]/d[CO]$ slopes ranged from 0.81 to 1.28 and averaged 1.0. During 2003, biomass burning emissions may have contributed to all events. However, the impact was apparently minimal during events 10 and 11, which do not exhibit correlated variations in CO and simulated AOT, and which include periods when all backward trajectories indicate flow from the south (e.g., Figure 4e shows trajectories arriving during a portion of event 11). These events also exhibited high slopes (averaging 0.97).

[49] Table 3 compares the PICO-NARE slopes with those from some of the prior studies summarized above. The Pico measurements differ in several ways from those in the other studies listed, and these differences may contribute to the higher slopes. Transport times to Pico during flow from the U.S. east coast averaged 5 to 6 days during USBL flow periods in 2001 and 2003. Applying the OH + CO rate constant (evaluated at 800 hPa [*Sander et al.*, 2003]) to an estimated average OH concentration of 2.8×10^6 molecules cm^{-3} (July zonal average at 800 hPa, 36°N [*Spivakovsky et al.*, 2000]), we estimate that CO mixing ratios would decline by 23–27% during that period. Adjusting the Pico measurements for this effect for comparison to eastern U.S. observations reduces the average slope of the 2001 and 2003 events (1.0) to 0.73. Alternatively, adjusting the Pico measurements for comparison with the slopes observed at Sable Island, which is itself about 2 days downwind of the eastern U.S. source regions, reduces the slope of 1.0 to 0.81. (Note that no adjustment for O$_3$ loss or production en-route is made here; net O$_3$ production will be assessed based on the slope comparison summarized in Table 3.)

[50] In addition, the other measurements summarized in Table 3 were obtained during the early 1990s. CO emissions over North America dropped significantly over the 1990s as a result of sharp declines in vehicular emissions [*Parrish et al.*, 2002], which *Parrish et al.* [2004] estimate resulted in a 20% reduction of U.S. CO emissions between 1990 and 2000. This change is apparent in CO levels observed in rural Virginia made between the late 1980s and late 1990s, which indicate a 2.5%/year decline in ambient CO [*Hallock-Waters et al.*, 1999]. Adjusting the 1991–

1994 slopes obtained at Sable Island for a 20% decline in CO enhancement (while maintaining the same O$_3$ enhancement) increases the June–August average Sable Island slope from 0.36 to 0.45.

[51] Thus, as summarized in Table 3, after accounting for CO loss during transport to the Azores and after accounting for a reduction in CO emissions in North America, the $d[O_3]/d[CO]$ slopes observed in North American outflow sampled at Pico are 80% higher than those observed in the Canadian maritime provinces (0.81 versus 0.45), and 90% higher than those observed in the eastern U.S. source region (0.73 versus 0.38).

[52] Although the motivation for analyzing the O$_3$-CO relationship is the deduction of the magnitude of ozone production, $d[O_3]/d[CO]$ slopes can vary for other reasons as well. First, the net amount of CO added to air flowing over the U.S. differs from the amount of CO emissions, due to CO production from hydrocarbon oxidation and CO loss by reaction with hydroxyl radical. Using model simulations, *Chin et al.* [1994] estimated that these two processes together result in an 18% increase in CO export from the eastern U.S. boundary layer during summer. It is unlikely that either process is the cause of the high slopes observed at Pico, however: continuing formation of CO from hydrocarbon oxidation in aging outflow would result in lower, not higher, $d[O_3]/d[CO]$ slopes, and we have adjusted the Pico slopes to account for the estimated CO loss downwind of North America.

[53] Second, dilution during transport in the absence of chemistry will lead to variations in CO and O$_3$ mixing ratios along a line connecting the original polluted airmass's composition with that of the diluent air. If the composition of the diluent air differs from that of the background air to which CO emissions and photochemically formed ozone were added, the slope will be changed. The potential impact of dilution during transport can be assessed by calculating the slope that would result from dilution of polluted eastern U.S. outflow with marine background air. To do this, we consider the dilution of air with the composition observed at Sable Island during outflow events during August (240 ppbv CO and 80 ppbv

O_3 [*Parrish et al.*, 1998, Figure 4]) or in elevated pollution layers in the same region (350 ppbv CO and 98 ppbv O_3 [*Daum et al.*, 1996, Figure 8]). As estimates of CO and O_3 mixing ratios in marine background air, we use the twentieth percentile of observations: 57 ppbv CO and 21 ppbv O_3 during 2001, and 75 ppbv CO and 26 ppbv O_3 during 2003. Together, these U.S. outflow and clean marine air endpoints define a slope of 0.26 to 0.32, much lower than observed at Pico. Adjusting the reported CO enhancements above background in eastern U.S. outflow by 20%, to simulate a 20% reduction in U.S. CO emissions, and by an additional 19%, to simulate CO loss during four more days of transport, increases the slopes expected from dilution alone to 0.40–0.49, values that are still much lower than the observed value of 1. Thus, dilution of continental outflow with clean marine air is not the cause of the high $d[O_3]/d[CO]$ slopes observed at Pico.

[54] To account for the ~75–80% higher than expected $d[O_3]/d[CO]$ slopes, then, significant additional CO loss, O_3 production, or O_3 input is required. We have already incorporated a 27% CO loss during 5–6 days of transport into this comparison. To explain the higher slope through an increased CO loss alone, an OH concentration ~3 times greater than assumed is required: 7.4×10^6 mol cm^{-3} as a 24-hour average. This seems unrealistically high, especially for transport occurring above the boundary layer. Alternatively, the cause may be an additional source of O_3. *Moody et al.* [1995] have noted the apparent importance of O_3 of upper tropospheric or stratospheric origin in U.S. outflow observed at Bermuda. However, those observations were made during spring and associated with rapid descent of air from the mid-troposphere following the passage of springtime low pressure systems. In contrast, most of the WAtl and USBL events discussed here do not exhibit subsidence (see, for example, Figures 4b, 4f, and 4h).

[55] A remaining possible explanation for the enhanced slope is the production of a significantly larger amount of ozone than occurred in the airmasses sampled over or near North America in the early 1990s. We suggest three mechanisms that should be evaluated further to determine whether they may have contributed significantly to the enhanced slope: continuing ozone formation during the 5–6 day travel time to the Azores, a decadal increase in the efficiency of ozone production over eastern North America, and differences in the types of airmasses sampled.

[56] The other studies summarized in Table 3 were conducted over or near eastern North America, and some degree of additional ozone production is expected during the additional several days of transport toward the Azores. However, *Li et al.* [2004] have estimated that the total amount of ozone formed in air exported away from the North American continent is only about 40% of that produced in or above the North American boundary layer, based on fall simulations with the GEOS-CHEM GCTM (this fraction is not expected to be significantly different during summer [*Liang et al.*, 1998]). Thus, the magnitude of downwind ozone production implied by the near doubling of the $d[O_3]/d[CO]$ slope is significantly greater than expected based on these model simulations. To better constrain this comparison, the ability of GCTMs to simulate the observed CO and O_3 enhancements in North American

plumes transported in the lower troposphere over the Azores needs to be evaluated.

[57] Evidence indicates that U.S. vehicular emissions of NO_x have increased since 1990 [*Parrish et al.*, 2002, 2004]. Much of the eastern U.S. is in the NO_x-sensitive ozone production regime [*Sillman*, 1999], and satellite measurements of formaldehyde and NO_2 columns indicate that this is especially true in the southeast U.S. [*Martin et al.*, 2004], a region over which many trajectories reaching the PICO-NARE station pass (e.g.., Figures 4a, 4c, 4e, 4g, and 4i). Increases in NO_x emissions in such an environment would result in an increase in the rate and ultimate magnitude of ozone production. Such an increase may have contributed to the increased slope observed in this study. If this is the case, then $d[O_3]/d[CO]$ slopes should have increased in the Canadian locations included in Table 3 as well; further measurements are needed to determine whether this is the case.

[58] A final possibility is that lower troposphere transport events over the Azores are associated with greater ozone production than are those that typically reach the Sable Island marine boundary layer site included in Table 3. The USBL-type events discussed here were typically associated with clear skies, and the backward trajectories imply transport in the lower free troposphere, where we expect the lifetimes of ozone and its precursors to be greater than in the marine boundary layer. In addition, there is some evidence that ozone production efficiency in air reaching Sable Island may be greater in events with maximum O_3 and CO levels similar to those in the events discussed here, in comparison to events with higher maximum CO and O_3 levels [*Parrish et al.*, 1998, Figure 6].

3.2.2. Biomass Burning Impacted Periods

[59] As noted above, the air sampled during most fire-influenced periods also passed over the northeast U.S. As a result, most of sampled plumes represent a mixture of anthropogenic and biomass burning emissions. In order to determine the ozone enhancement associated with long-range transport of biomass burning plumes to the station, we focus here on the four events that do not have significant anthropogenic influence: 2001 events 8 and 9, and 2003 events 12 and 13. Backward trajectories arriving during these events consistently travelled over sparsely populated regions of Canada, and did not pass over the U.S. or high-emission regions of Canada (or, in the case of 2001 event 9, did not do so during a portion of the period of high-CO observations). Each of these events is attributed to long-range transport of emissions from Siberian fires, which travelled for ~13–15 days before reaching the Azores.

[60] Ozone mixing ratios increased significantly during these events, rising by 15–35 ppbv. CO and O_3 were less well correlated ($r^2 = 0.4$ to 0.5) than during most U.S. outflow events. As a result, the slopes, which range from 0.4 to 0.9 (ppbv O_3/ppbv CO) have much higher relative uncertainty (~50%). We suggest that this was a result of the much longer transport period from Siberia than from the eastern U.S., which provides the opportunity for other processes to alter CO and O_3 mixing ratios, by mixing and photochemical or depositional losses. To provide an alternative characterization of the relative O_3 and CO enhancements associated with long-range transport of these Siberian fire plumes not based on regression results,

we have also calculated mean values of $\Delta[O_3]/\Delta[CO]$ for all observations during each event when CO was elevated by more than 20 ppbv above background, where $\Delta[O_3] = [O_3] - [O_3]_{background}$, and $\Delta[CO]$ is defined similarly. For background values, we used the low-CO mode each year (61 ppbv in 2001 and 80 ppbv in 2003) for CO and 25 ppbv for O_3. The resulting enhancement ratios (mean ± 2 standard errors) are 0.93 ± 0.04 for 2001 event 8, 0.84 ± 0.14 for 2001 event 9, 0.45 ± 0.02 for 2003 event 12, and 0.61 ± 0.04 for 2003 event 13. These ratios are similar in magnitude to the regression slopes.

[61] These ozone enhancement ratios (and the corresponding slopes) are smaller than the slopes derived for most of the events with anthropogenic influence only. This is consistent with earlier studies of boreal biomass burning plumes, which have shown that high-latitude biomass burning plumes exhibit regression slopes significantly lower than those for urban and industrial pollution. These lower slopes have been attributed to lower NO_x:CO emission ratios, relative to that of urban and industrial emissions [*Jacob et al.*, 1992; *Goode et al.*, 2000; *Andreae et al.*, 1994], and to rapid conversion of NO_x to peroxyacetyl nitrate (PAN) at the lower temperatures present at high latitudes [*Jacob et al.*, 1992].

[62] However, the O_3 enhancement ratios we report here are higher than those reported previously for aged boreal fire plumes, which are generally below 0.2 [*Wotawa and Trainer*, 2000; *Wofsy et al.*, 1992; *McKeen et al.*, 2002]. This may reflect loss of CO and production of O_3 during the very long transport times in these events. CO loss of as much as 50% is expected during the $\sim 13-15$ day transport period, and this alone would double $\Delta[O_3]/\Delta[CO]$ ratios. In addition, CO oxidation results in the production of hydroperoxy radical; the resulting impact on ozone is sensitive to NO concentrations, and may be either positive or negative. In the presence of sufficient NO, this amount of CO oxidation would lead to the production of a significant amount of O_3. Although NO_x concentrations in moderately aged boreal fire plumes are low, NO_y concentrations are large, with a significant (one-third or more) contribution of PAN [*Wofsy et al.*, 1992], as a result of rapid conversion to PAN during the first day downwind [*Jacob et al.*, 1992; *Trentmann et al.*, 2003]. Subsidence-induced warming during transport southward to the latitude of the Azores may have resulted in PAN decomposition, releasing NO_x and allowing continuing O_3 production.

[63] Although there are few observations in such highly aged biomass burning plumes, prior measurements have demonstrated continuing ozone formation in aging plumes. For example, *Yokelson et al.* [2003] sampled fresh and moderately aged tropical biomass burning plumes, and found $\Delta[O_3]/\Delta[CO]$ ratios that increased from 0.09 after 1 hour to 0.22 in 2–4 day-old plumes. Older tropical plumes were analyzed by *Mauzerall et al.* [1998], who found that enhancement ratios increased from 0.15 in fresh plumes to more than 0.7 in plumes 5–7 days old; similarly large enhancement ratios in aged tropical plumes have been reported in a limited number of additional plume observations [*Andreae et al.*, 1994; *Singh et al.*, 2000]. In the North Atlantic region, *Forster et al.* [2001] sampled a plume from Canadian fires that reached the free troposphere over Europe in August 1998. Although CO was not mea-

sured, the observed ozone enhancement was 20–25 ppbv, similar to that observed in this work.

[64] Since the backward trajectories arriving during these events subsided from altitudes of approximately 4–5 km, a contribution from upper tropospheric or stratospheric ozone is also possible. However, the observed correlation with CO and the long duration of elevated and correlated CO and O_3 (during 2003 event 12) lead us to believe that such an impact is not dominant.

4. Conclusions

[65] Enhancements of CO levels above the marine background level were frequently observed at the PICO-NARE station during the summers of 2001–2003. An analysis of backward trajectories arriving in the lower free troposphere demonstrated that nearly all periods of elevated CO are attributable to either North American pollution outflow or long-range transport of biomass burning emissions. (Backward trajectories travelling in the marine boundary layer and arriving at the times of elevated CO observations generally did not travel over pollution source regions, consistent with our expectation that the PICO-NARE station most often samples free tropospheric air.)

[66] The highest CO levels all occurred during periods apparently impacted by fire emissions. Very high Siberian fire activity in 2003 and impacts from a Canadian fire in 2002, in combination with interannual variability in the frequency of transport from the subarctic, apparently caused higher CO levels during 2002, and much higher CO levels in 2003, than in 2001. The major impact of biomass burning emissions at the Azores station, especially those from distant Siberian fires, demonstrates the important contribution of boreal biomass burning to background CO in the northern hemisphere. Ozone mixing ratios were also elevated during periods of biomass burning impacts. The occurrence of increased ozone mixing ratios after more than 10 days of transport from Siberian fires implies a significant impact of such fires on northern hemispheric ozone as well, and the magnitude of this enhancement suggests continuing ozone formation in highly aged plumes.

[67] Ozone and CO mixing ratios were highly correlated in flow from the eastern U.S. when biomass burning impacts were absent. The slope ($d[O_3]/d[CO]$) averaged 1.0 (ppbv/ppbv) during such periods, a value that is at least 80% larger than previously observed in the eastern U.S. and nearby downwind regions, even after accounting for declining U.S. CO emissions and CO oxidation en-route to the Azores. We were unable to explain the observed slopes as the result of airmass mixing. They therefore suggest a significantly increased amount of net ozone production. We hypothesize three mechanisms that may have contributed to this, and suggest further work needed to evaluate them. They include the production of an amount of additional O_3 formation during transport to the Azores that is significantly greater than expected based on model simulations, a significant increase in O_3 production over the eastern U.S. and the nearby downwind regions resulting from increased NO_x emissions since the early 1990s, and enhanced ozone production resulting from emissions carried in relatively slow-moving air travelling in the lower troposphere under clear-sky conditions. Each of these, if

the actual cause, could imply that current estimates of the impact of North American emissions on the hemispheric O_3 budget are significant underestimates. Additional measurements within lower tropospheric U.S. outflow are needed to determine whether the high slopes observed in this study indeed reflect enhanced O_3 production as we have concluded they do, and, if so, to determine the cause.

References

Albrecht, B. A., C. Bretherton, D. Johnson, W. Scubert, and A. Frisch (1995), The Atlantic Stratocumulus Transition Experiment—ASTEX, *Bull. Am. Meteorol. Soc.*, *76*, 889–904.

Anderson, B. E., J. E. Collins, G. W. Sachse, G. W. Whiting, D. R. Blake, and F. S. Rowland (1993), AASE-II observations of trace carbon species distributions in the mid to upper troposphere, *Geophys. Res. Lett.*, *20*, 2539–2542.

Andreae, M. O., B. E. Anderson, D. R. Blake, J. D. Bradshaw, J. E. Collins, G. L. Gregory, G. W. Sachse, and M. C. Shipham (1994), Influence of plumes from biomass burning on atmospheric chemistry over the equatorial and tropical South Atlantic during CITE 3, *J. Geophys. Res.*, *99*, 12,793–12,808.

Ayers, G. (2001), Comment on regression analysis of air quality data, *Atmos. Environ.*, *35*, 2423–2425.

Banic, C. M., W. R. Leaitch, G. A. Isaac, M. D. Couture, L. I. Kleinman, S. R. Springston, and J. I. MacPherson (1996), Transport of ozone and sulfur to the North Atlantic atmosphere during the North Atlantic Regional Experiment, *J. Geophys. Res.*, *101*, 29,091–29,104.

Chin, M., D. J. Jacob, J. W. Munger, D. D. Parrish, and B. G. Doddridge (1994), Relationship of ozone and carbon monoxide over North America, *J. Geophys. Res.*, *99*, 14,565–14,573.

Christensen, J. H. (1997), The Danish eulerian hemispheric model - A three-dimensional air pollution model used for the Arctic, *Atmos. Environ.*, *31*, 4169–4191.

Colarco, P. R., M. R. Schoeberl, B. G. Doddridge, L. T. Marufu, O. Torres, and E. J. Welton (2004), Transport of smoke from Canadian forest fires to the surface near Washington, D. C.: Injection height, entrainment, and optical properties, *J. Geophys. Res.*, *109*, D06203, doi:10.1029/2003JD004248.

Cooper, O. R., et al. (2001), Trace gas signatures of the airstreams within North Atlantic cyclones: Case studies from the North Atlantic Regional Experiment (NARE'97) aircraft intensive, *J. Geophys. Res.*, *106*, 5437–5456.

Daum, P. H., L. I. Kleinman, L. Newman, W. T. Luke, J. Weinstein-Lloyd, and C. M. Berkowitz (1996), Chemical and physical properties of plumes of anthropogenic pollutants transported over the North Atlantic during the North Atlantic Regional Experiment, *J. Geophys. Res.*, *101*, 29,029–29,042.

Dickerson, R. R., B. G. Doddridge, and P. Kelley (1995), Large-scale pollution of the atmosphere over the remote Atlantic Ocean: Evidence from Bermuda, *J. Geophys. Res.*, *100*, 8945–8952.

Ding, L., R. J. Calhoun, and R. L. Street (2003), Numerical simulation of strongly stratified flow over a three-dimensional hill, *Boundary Layer Meteorol.*, *107*, 81–114.

Draper, N. R., and H. Smith (1998), *Applied Regression Analysis*, John Wiley, Hoboken, N. J.

Draxler, R., and G. Rolph (2003), HYSPLIT4 (HYbrid Single-Particle Lagrangian Integrated Trajectory) model, Air Resour. Lab., Natl. Oceanic and Atmos. Admin., Silver Spring, Md. (Available at http://www.arl.noaa.gov/ready/hysplit4.html)

Eck, T. F., B. N. Holben, J. Reid, N. T. O'Neill, J. S. Schafer, O. Dubovik, A. Smirnov, M. Yamasoe, and P. Artaxo (2003), High aerosol optical depth biomass burning events: A comparison of optical properties for different source regions, *Geophys. Res. Lett.*, *30*(20), 2035, doi:10.1029/2003GL017861.

Eckhardt, S., A. Stohl, H. Wernli, P. James, C. Forster, and N. Spichtinger (2004), A 15-year climatology of warm conveyor belts, *J. Clim.*, *17*, 218–236.

Edwards, D. P., et al. (2004), Observations of carbon monoxide and aerosols from the Terra satellite: Northern Hemisphere variability, *J. Geophys. Res.*, *109*, D24202, doi:10.1029/2004JD004727.

Forster, C., et al. (2001), Transport of boreal forest fire emissions from Canada to Europe, *J. Geophys. Res.*, *106*, 22,887–22,906.

Fowler, D. (1999), The global exposure of forests to air pollutants, *Water Air Soil Pollut.*, *116*(1), 5–32.

Goode, J. G., R. J. Yokelson, D. E. Ward, R. A. Susott, R. E. Babbitt, M. A. Davies, and W. M. Hao (2000), Measurements of excess O_3, CO, CO_2, CH_4, C_2H_6, C_2H_4, HCN, NO, NH_3, HCOOH, CH_3COOH, HCHO, and CH_3OH in 1997 Alaskan biomass burning plumes by airborne Fourier transform infrared spectroscopy (AFTIR), *J. Geophys. Res.*, *105*, 22,147–22,166.

Hallock-Waters, K. A., B. G. Doddridge, R. R. Dickerson, S. Spitzer, and J. D. Ray (1999), Carbon monoxide in the U.S. Mid-Atlantic troposphere: Evidence for a decreasing trend, *Geophys. Res. Lett.*, *26*, 2861–2864.

Hoell, J. M., D. D. Davis, S. C. Liu, R. E. Newell, H. Akimoto, R. J. McNeal, and R. J. Bendura (1997), The Pacific Exploratory Mission-West Phase B: February–March, 1994, *J. Geophys. Res.*, *102*, 28,223–28,249.

Hogan, T. F., and L. R. Brody (1991), Sensitivity studies of the Navy's global forecast model parameterizations and evaluation of improvements to NOGAPS, *Mon. Weather Rev.*, *121*, 2373–2395.

Houghton, J. T., Y. Ding, D. J. Griggs, M. Noguer, P. J. van der Linden, X. Dai, K. Maskell, and C. A. Johnson (2001), *Climate Change 2001: The Scientific Basis—Contribution of Working Group I to the Third Assessment Report of the Intergovernmental Panel on Climate Change*, Cambridge Univ. Press, New York.

Jacob, D. J., et al. (1992), Summertime photochemistry of the troposphere at high northern latitudes, *J. Geophys. Res.*, *97*, 16,421–16,431.

Jacob, D. J., et al. (2003), Transport and Chemical Evolution over the Pacific (TRACE-P) aircraft mission: Design, execution, and first results, *J. Geophys. Res.*, *108*(D20), 9000, doi:10.1029/2002JD003276.

Jaffe, D., et al. (1999), Transport of Asian air pollution to North America, *Geophys. Res. Lett.*, *26*, 711–714.

Jaffe, D., I. Bertschi, L. Jaeglé, P. Novelli, J. S. Reid, H. Tanimoto, R. Vingarzan, and D. L. Westphal (2004), Long-range transport of Siberian biomass burning emissions and impact on surface ozone in western North America, *Geophys. Res. Lett.*, *31*, L16106, doi:10.1029/2004GL020093.

Justice, C. O., et al. (2002), The MODIS fire products, *Remote Sens. Environ.*, *83*, 244–262.

Li, Q., D. J. Jacob, J. W. Munger, R. M. Yantosca, and D. D. Parrish (2004), Export of NO_y from the North American boundary layer: Reconciling aircraft observations and global model budgets, *J. Geophys. Res.*, *109*, D02313, doi:10.1029/2003JD004086.

Liang, J., L. W. Horowitz, D. J. Jacob, Y. Wang, A. M. Fiore, J. A. Logan, G. M. Gardner, and J. W. Munger (1998), Seasonal budgets of reactive nitrogen species and ozone over the United States and export fluxes to the global atmosphere, *J. Geophys. Res.*, *103*, 13,435–13,450.

Martin, R. V., A. M. Fiore, and A. Van Donkelaar (2004), Space-based diagnosis of surface ozone sensitivity to anthropogenic emissions, *Geophys. Res. Lett.*, *31*, L06120, doi:10.1029/2004GL019416.

Mauzerall, D. L., and X. Wang (2001), Protecting agricultural crops from the effects of tropospheric ozone exposure: Reconciling science and standard setting in the United States, Europe, and Asia, *Annu. Rev. Energy Environ.*, *26*, 237–268.

Mauzerall, D. L., et al. (1998), Photochemistry in biomass burning plumes and implications for tropospheric ozone over the tropical South Atlantic, *J. Geophys. Res.*, *103*, 8401–8423.

McKeen, S. A., G. Wotawa, D. D. Parrish, J. S. Holloway, M. P. Buhr, G. Hübler, F. C. Fehsenfeld, and J. F. Meagher (2002), Ozone production from Canadian wildfires during June and July of 1995, *J. Geophys. Res.*, *107*(D14), 4192, doi:10.1029/2001JD000697.

Mendonca, B. G. (1969), Local wind circulation on the slopes of Mauna Loa, *J. Appl. Meteorol.*, 533–541.

Merrill, J. T. (1994), Isentropic airflow probability analysis, *J. Geophys. Res.*, *99*, 25,881–25,889.

Moody, J. L., S. J. Oltmans, H. Levy II, and J. T. Merrill (1995), Transport climatology of tropospheric ozone: Bermuda, 1988–1991, *J. Geophys. Res.*, *100*, 7179–7194.

Moody, J. L., J. W. Munger, A. H. Goldstein, D. J. Jacob, and S. C. Wofsy (1998), Harvard Forest regional-scale air mass composition by Patterns in Atmospheric Transport History (PATH), *J. Geophys. Res.*, *103*, 13,181–13,194.

Novelli, P. C., K. A. Masarie, P. M. Lang, B. D. Hall, R. C. Myers, and J. W. Elkins (2003), Reanalysis of tropospheric CO trends: Effects of the 1997–1998 wildfires, *J. Geophys. Res.*, *108*(D15), 4464, doi:10.1029/2002JD003031.

Pahlow, M., J. Kleissl, M. B. Parlange, J. M. Ondov, and D. Harrison (2004), Atmospheric boundary-layer structure observed during a haze event due to forest-fire smoke, *Boundary Layer Meteorol.*, in press.

Parrish, D. D., C. J. Hahn, E. J. Williams, R. B. Norton, F. C. Fehsenfeld, H. B. Singh, J. D. Shetter, B. W. Gandrud, and B. A. Ridley (1992), Indications of photochemical histories of Pacific air masses from measurements of atmospheric trace species at Point Arena, California, *J. Geophys. Res.*, *97*, 15,883–15,901.

Parrish, D. D., J. S. Holloway, M. Trainer, P. C. Murphy, G. L. Forbes, and F. C. Fehsenfeld (1993), Export of North American ozone pollution to the North Atlantic Ocean, *Science*, *259*, 1436–1439.

Parrish, D. D., J. S. Holloway, and F. C. Fehsenfeld (1994), Routine, continuous measurement of carbon monoxide with parts per billion precision, *Environ. Sci. Technol.*, *28*, 1615–1618.

Parrish, D. D., M. Trainer, J. S. Holloway, J. E. Yee, M. S. Warshawsky, F. C. Fehsenfeld, G. Forbes, and J. L. Moody (1998), Relationships between ozone and carbon monoxide at surface sites in the North Atlantic region, *J. Geophys. Res.*, *103*, 13,357–13,376.

Parrish, D. D., M. Trainer, E. J. Williams, K. J. Olszyna, R. A. Harley, J. F. Meagher, and F. C. Fehsenfeld (2002), Decadal change in carbon monoxide to nitrogen oxide ratio in U.S. vehicular emissions, *J. Geophys. Res.*, *107*(D12), 4140, doi:10.1029/2001JD000720.

Parrish, D. D., et al. (2004), Fraction and composition of NO$_y$ transported in air masses lofted from the North American boundary layer, *J. Geophys. Res.*, *109*, D09302, doi:10.1029/2003JD004226.

Paton-Walsh, C., N. Jones, S. Wilson, A. Meier, N. Deutscher, D. Griffith, R. Mitchell, and S. Campbell (2004), Trace gas emissions from biomass burning inferred from aerosol optical depth, *Geophys. Res. Lett.*, *31*, L05116, doi:10.1029/2003GL018973.

Peterson, M. C., R. E. Honrath, D. D. Parrish, and S. J. Oltmans (1998), Measurements of nitrogen oxides and a simple model of NO$_y$ fate in the remote North Atlantic marine atmosphere, *J. Geophys. Res.*, *103*, 13,489–13,503.

Pochanart, P., H. Akimoto, Y. Kajii, V. M. Potemkin, and T. V. Khodzher (2003), Regional background ozone and carbon monoxide variations in remote Siberia/East Asia, *J. Geophys. Res.*, *108*(D1), 4028, doi:10.1029/2001JD001412.

Poirot, R. L., and P. R. Wishinski (1986), Visibility, sulfate and air mass history associated with the summertime aerosol in northern Vermont, *Atmos. Environ.*, *20*, 1457–1469.

Prins, E., J. M. Feltz, W. P. Menzel, and D. E. Ward (1998), An overview of GOES-8 diurnal fire and smoke results for SCAR-B and the 1995 fire season in South America, *J. Geophys. Res.*, *103*, 31,821–31,836.

Prins, E., J. Schmetz, L. Flynn, D. Hillger, and J. Feltz (2001), Overview of current and future diurnal active fire monitoring using a suite of international geostationary satellites, in *Global and Regional Wildfire Monitoring: Current Status and Future Plans*, edited by F. J. Ahern, J. G. Goldammer, and C. O. Justice, pp. 145–170, SPB Acad., The Hague, Netherlands.

Prins, E., C. Schmidt, J. Feltz, J. Reid, D. Westphal, and K. Richardson (2003), A two-year analysis of fire activity in the Western Hemisphere as observed with the GOES Wildfire Automated Biomass Burning Algorithm, paper presented at 12th Conference on Satellite Meteorology and Oceanography, Am. Meteorol. Soc., Long Beach, Calif.

Reid, J. S., R. Koppmann, T. F. Eck, and D. P. Eleuterio (2004a), A review of biomass burning emissions part II: Intensive physical properties of biomass burning particles, *Atmos. Chem. Phys. Discuss.*, *4*, 5135–5200.

Reid, J. S., et al. (2004b), Real-time monitoring of South American smoke particle emissions and transport using a coupled remote sensing/box-model approach, *Geophys. Res. Lett.*, *31*, L06107, doi:10.1029/2003GL018845.

Sander, S. P., et al. (2003), Chemical kinetics and photochemical data for use in atmospheric studies, Evaluation 14, *JPL Publ., 02-25*.

Sillman, S. (1999), The relation between ozone, NO$_x$ and hydrocarbons in urban and polluted rural environments, *Atmos. Environ.*, *33*, 1821–1845.

Singh, H. B., et al. (2000), Biomass burning influences on the composition of the remote South Pacific troposphere: Analysis based on observations from PEM-Tropics-A, *Atmos. Environ.*, *34*, 635–644.

Spivakovsky, C. M., et al. (2000), Three-dimensional climatological distribution of tropospheric OH: Update and evaluation, *J. Geophys. Res.*, *105*, 8931–8980.

Stohl, A., M. Trainer, T. B. Ryerson, J. S. Holloway, and D. D. Parrish (2002), Export of NO$_y$ from the North American boundary layer during 1996 and 1997 North Atlantic Regional Experiments, *J. Geophys. Res.*, *107*(D11), 4131, doi:10.1029/2001JD000519.

Stunder, B. J. B. (1997), NCEP model output—FNL archive data, *Tech. Rep. TD-6141*, Air Resour. Lab., Natl. Oceanic and Atmos. Admin., Silver Spring, Md. (Available at http://www.arl.noaa.gov/ready-bin/fnl.pl)

Thompson, A. M. (1992), The oxidizing capacity of the Earth's atmosphere: Probable past and future changes, *Science*, *256*, 1157–1165.

Trentmann, J., M. Andreae, and H.-F. Graf (2003), Chemical processes in a young biomass-burning plume, *J. Geophys. Res.*, *108*(D22), 4705, doi:10.1029/2003JD003732.

Trickl, T., O. R. Cooper, H. Eisele, P. James, R. Mücke, and A. Stohl (2003), Intercontinental transport and its influence on the ozone concentrations over Europe: Three case studies, *J. Geophys. Res.*, *108*(D12), 8530, doi:10.1029/2002JD002735.

Wofsy, S. C., et al. (1992), Atmospheric chemistry in the Arctic and subarctic: Influence of natural fires, industrial emissions, and stratospheric inputs, *J. Geophys. Res.*, *97*, 16,731–16,746.

Wotawa, G., and M. Trainer (2000), The influence of Canadian forest fires on pollutant concentrations in the United States, *Science*, *288*, 324–328.

Wotawa, G., P. C. Novelli, M. Trainer, and C. Granier (2001), Inter-annual variability of summertime CO concentrations in the northern hemisphere explained by boreal forest fires in North America and Russia, *Geophys. Res. Lett.*, *28*, 4575–4578.

Yokelson, R. J., I. T. Bertschi, T. J. Christian, P. V. Hobbs, D. E. Ward, and W. M. Hao (2003), Trace gas measurements in nascent, aged, and cloud-processed smoke from African savanna fires by airborne fourier transform infrared spectroscopy (AFTIR), *J. Geophys. Res.*, *108*(D13), 8478, doi:10.1029/2002JD002322.

————————

M. P. Dziobak, R. E. Honrath, J. Kleissl, K. Lapina, R. C. Owen, and M. Val Martín, Department of Civil and Environmental Engineering, Michigan Technological University, Houghton, MI 49931-1295, USA. (reh@mtu.edu)

P. Fialho, Group of Chemistry and Physics of the Atmosphere, University of the Azores, PT9701-851 Angra do Heroismo, Portugal.

J. S. Reid and D. L. Westphal, Marine Meteorology Division, Naval Research Laboratory, Monterey, CA 93943, USA.
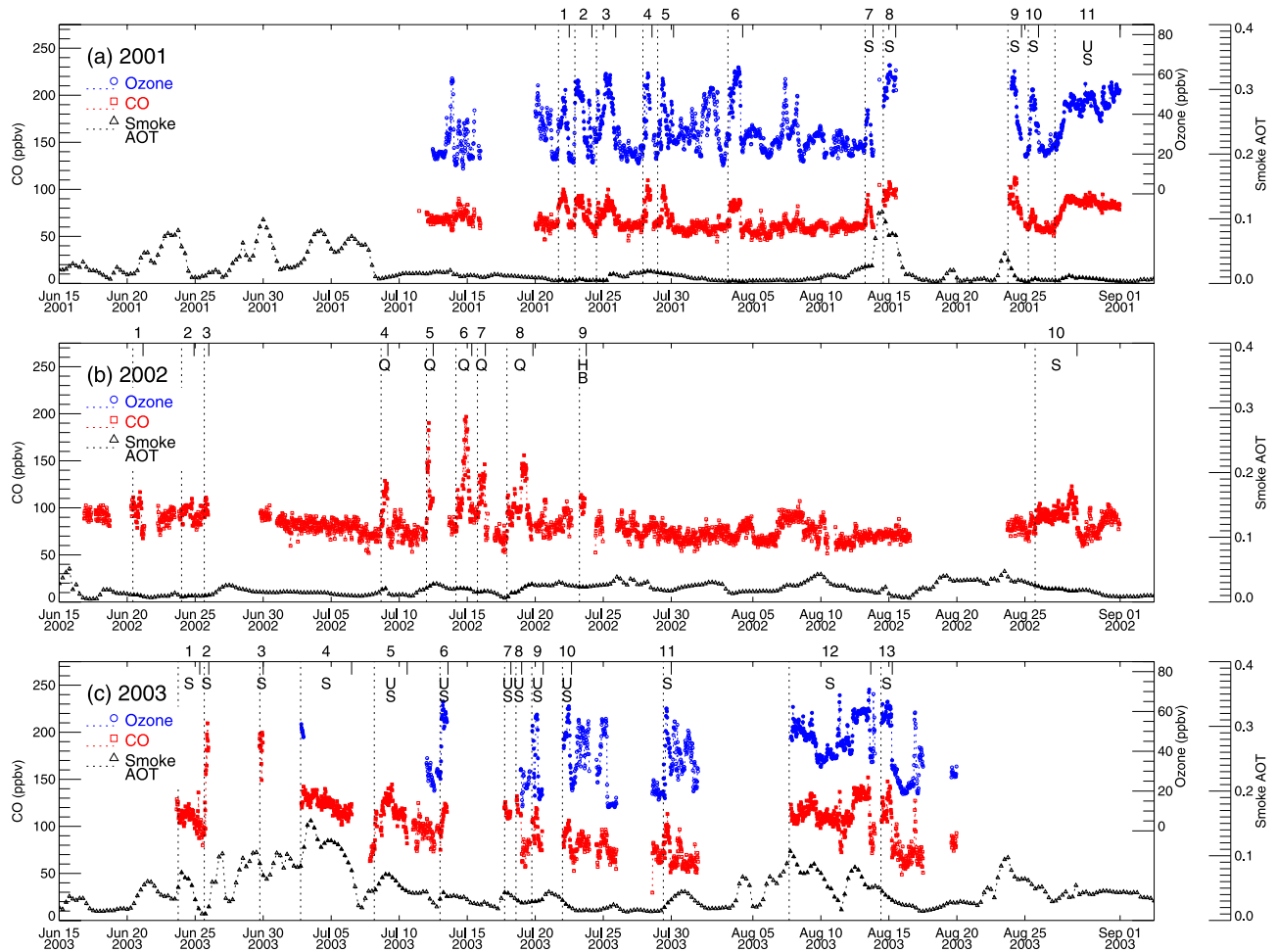
Figure 1. Time series of measured CO, measured O$_3$, and NAAPS/FLAMBE smoke aerosol optical thickness (AOT) each summer. CO is plotted with red squares, ozone is plotted with blue circles, and smoke AOT is plotted with black triangles. (Ozone measurements are not available during summer 2002, and are missing during some periods in 2003.) Events discussed in the text begin at the dotted vertical lines, end at the solid vertical lines, and are numbered above each plot; values during these events are plotted with solid symbols. Source-fire regions for biomass burning-impacted periods (discussed in section 3.1.2) are identified near the top of each plot: S, Siberia; Q, Quebec; HB, Hudson Bay; US, the western United States.
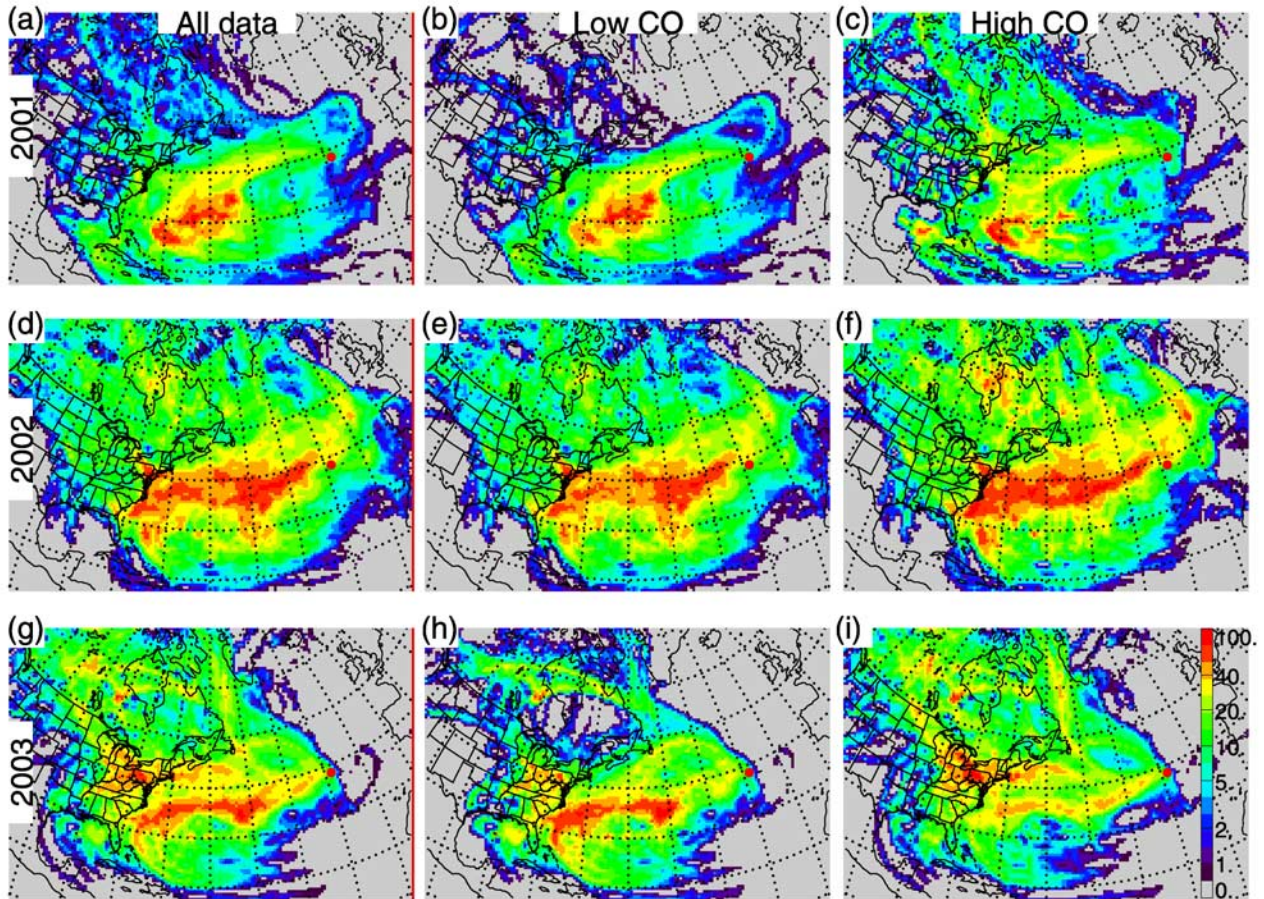
Figure 3. Residence time plots for (a, d, g) all data each summer, (b, e, h) low-CO periods (see text for definition), and (c, f, i) high-CO periods (see text for definition) during (a, b, c) 2001, (d, e, f) 2002, and (g, h, i) 2003. Color scale (shown in Figure 3i) is normalized to the highest geometrically corrected residence time value in each data subset.
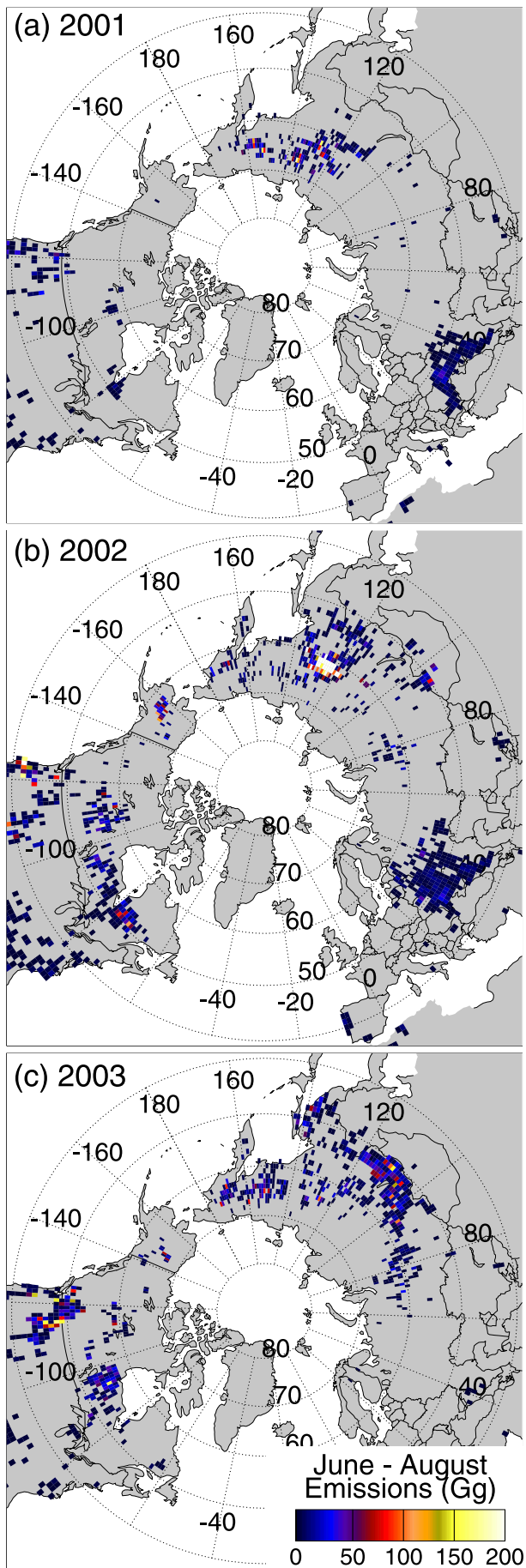
Figure 5. The spatial patterns of summertime biomass burning aerosol particle emissions during (a) 2001, (b) 2002, and (c) 2003 from the real-time FLAMBE emission model.
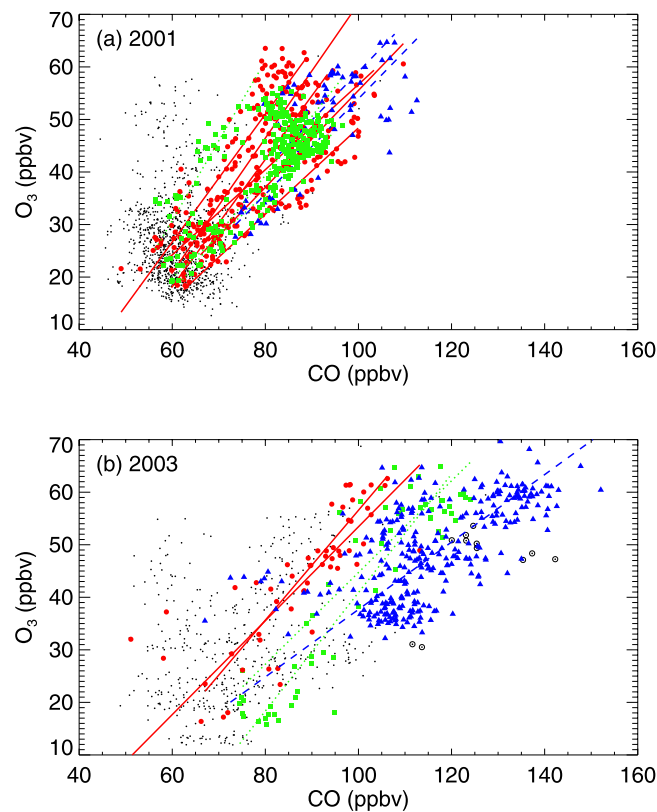
Figure 7. Relationship between CO and O_3 during (a) 2001 and (b) 2003 (O_3 measurements during 2002 are not available). Measurements obtained during periods outside of the events listed in Table 1 are plotted with small black dots. Observations obtained during the events listed in Table 1 are plotted with larger symbols, and regression lines are shown for those events with slope uncertainty below 50%. Symbols and lines are coded according to each event's identified source region and the potential for biomass burning influence, as follows: solid red circles and red solid lines: USBL with no or minimal biomass burning influence (2001 events 1–6, 2003 events 10–11; see text); solid blue triangles and blue dashed lines: biomass burning-influenced periods (not USBL) (2001 events 8–9, 2003 events 12–13); solid green squares and green dotted lines: other (mixed influence) (2001 events 7 and 10–11, 2003 events 6 and 9); and measurements during the small fractions of 2003 events 4 and 8 for which ozone measurements were made: open black circles.